The Astrophysical Journal, 908:143 (24pp), 2021 February 20 https://doi.org/10.3847/1538-4357/abd7f5
© 2021. The American Astronomical Society. All rights reserved.

The Young Supernova Experiment: Survey Goals, Overview, and Operations

D. O. Jones[1,22], R. J. Foley[1], G. Narayan[2,3], J. Hjorth[4], M. E. Huber[5], P. D. Aleo[2,3], K. D. Alexander[6,22], C. R. Angus[4], K. Auchettl[1,4,7,8], V. F. Baldassare[9], S. H. Bruun[4], K. C. Chambers[5], D. Chatterjee[2,3], D. L. Coppejans[6], D. A. Coulter[1], L. DeMarchi[6], G. Dimitriadis[1], M. R. Drout[10], A. Engel[2,3], K. D. French[2,3,11,23], A. Gagliano[2,3], C. Gall[4], T. Hung[1], L. Izzo[4], W. V. Jacobson-Galán[6], C. D. Kilpatrick[1], H. Korhonen[4,12], R. Margutti[6], S. I. Raimundo[4,13], E. Ramirez-Ruiz[1,4], A. Rest[14,15], C. Rojas-Bravo[1], M. R. Siebert[1], S. J. Smartt[16], K. W. Smith[16], G. Terreran[6], Q. Wang[14], R. Wojtak[4], A. Agnello[4], Z. Ansari[4], N. Arendse[4], A. Baldeschi[6], P. K. Blanchard[6], D. Brethauer[6], J. S. Bright[6], J. S. Brown[1], T. J. L. de Boer[5], S. A. Dodd[1], J. R. Fairlamb[5], C. Grillo[4,17], A. Hajela[6], C. Hede[4], A. N. Kolborg[4], J. A. P. Law-Smith[1], C.-C. Lin[5], E. A. Magnier[5], K. Malanchev[2,18], D. Matthews[6], B. Mockler[1,4], D. Muthukrishna[19], Y.-C. Pan[20], H. Pfister[4,21], D. K. Ramanah[4], S. Rest[14], A. Sarangi[4], S. L. Schrøder[4], C. Stauffer[6], M. C. Stroh[6], K. L. Taggart[1], S. Tinyanont[1], and R. J. Wainscoat[5]

(Young Supernova Experiment)

[1] Department of Astronomy and Astrophysics, University of California, Santa Cruz, CA 95064, USA; david.jones@ucsc.edu
[2] Department of Astronomy, University of Illinois at Urbana-Champaign, 1002 W. Green St., IL 61801, USA
[3] Center for Astrophysical Surveys, National Center for Supercomputing Applications, Urbana, IL 61801, USA
[4] DARK, Niels Bohr Institute, University of Copenhagen, Jagtvej 128, 2200 Copenhagen, Denmark
[5] Institute for Astronomy, University of Hawaii, 2680 Woodlawn Drive, Honolulu, HI 96822, USA
[6] Center for Interdisciplinary Exploration and Research in Astrophysics (CIERA) and Department of Physics and Astronomy, Northwestern University, Evanston, IL 60208, USA
[7] School of Physics, The University of Melbourne, VIC 3010, Australia
[8] ARC Centre of Excellence for All Sky Astrophysics in 3 Dimensions (ASTRO 3D), Australia
[9] Department of Physics & Astronomy, Washington State University, Pullman, WA 99164, USA
[10] David A. Dunlap Department of Astronomy and Astrophysics, University of Toronto, 50 St. George Street, Toronto, ON M5S 3H4, Canada
[11] Observatories of the Carnegie Institute for Science, 813 Santa Barbara St., Pasadena, CA 91101, USA
[12] European Southern Observatory, Alonso de Córdova 3107, Vitacura, Santiago, Chile
[13] Department of Physics and Astronomy, University of Southampton, Highfield, Southampton SO17 1BJ, UK
[14] Department of Physics and Astronomy, The Johns Hopkins University, Baltimore, MD 21218, USA
[15] Space Telescope Science Institute, Baltimore, MD 21218, USA
[16] Astrophysics Research Centre, School of Mathematics and Physics, Queen's University Belfast, Belfast BT7 1NN, UK
[17] Dipartimento di Fisica, Università degli Studi di Milano, via Celoria 16, I-20133 Milano, Italy
[18] Sternberg Astronomical Institute, Lomonosov Moscow State University 13 Universitetsky pr., Moscow 119234, Russia
[19] Institute of Astronomy and Kavli Institute for Cosmology, Madingley Road, Cambridge, CB3 0HA, UK
[20] Graduate Institute of Astronomy, National Central University, 300 Zhongda Road, Zhongli, Taoyuan 32001, Taiwan
[21] Department of Physics, The University of Hong Kong, Pokfulam Road, Hong Kong, People's Republic of China
Received 2020 October 14; revised 2020 December 17; accepted 2020 December 30; published 2021 February 19

Abstract

Time-domain science has undergone a revolution over the past decade, with tens of thousands of new supernovae (SNe) discovered each year. However, several observational domains, including SNe within days or hours of explosion and faint, red transients, are just beginning to be explored. Here we present the Young Supernova Experiment (YSE), a novel optical time-domain survey on the Pan-STARRS telescopes. Our survey is designed to obtain well-sampled *griz* light curves for thousands of transient events up to $z \approx 0.2$. This large sample of transients with four-band light curves will lay the foundation for the Vera C. Rubin Observatory and the Nancy Grace Roman Space Telescope, providing a critical training set in similar filters and a well-calibrated low-redshift anchor of cosmologically useful SNe Ia to benefit dark energy science. As the name suggests, YSE complements and extends other ongoing time-domain surveys by discovering fast-rising SNe within a few hours to days of explosion. YSE is the only current four-band time-domain survey and is able to discover transients as faint as ∼21.5 mag in *gri* and ∼20.5 mag in *z*, depths that allow us to probe the earliest epochs of stellar explosions. YSE is currently observing approximately 750 deg^2 of sky every 3 days, and we plan to increase the area to 1500 deg^2 in the near future. When operating at full capacity, survey simulations show that YSE will find ∼5000 new SNe per year and at least two SNe within 3 days of explosion per month. To date, YSE has discovered or observed 8.3% of the transient candidates reported to the International Astronomical Union in 2020. We present an overview of YSE, including science goals, survey characteristics, and a summary of our transient discoveries to date.

Unified Astronomy Thesaurus concepts: Supernovae (1668); Cosmology (343); Sky surveys (1464); Transient detection (1957)

[22] NASA Einstein Fellow.
[23] Hubble Fellow.

1. Introduction

For thousands of years, astrophysical transients were discovered only by chance. It was Zwicky (1938) who began the first systematic search for extragalactic astrophysical transients, which evolved into the Palomar Supernova Search, discovering over 100 supernovae (SNe) in the following few decades. Systematic searches of the southern sky started in the 1980s (Maza 1980), essentially doubling capabilities. Combining charge-coupled devices (CCDs) with robotic telescopes to automatically search for SNe was the next major innovation (Kare et al. 1982), although successful searches started about a decade after initial tries (Perlmutter 1989; Filippenko 1992; Richmond et al. 1993).

The discovery of SN 1987A (Kunkel et al. 1987) caused a resurgence of interest in SN science, and at a similar time, advances in calibrating SNe Ia, building on the work of Kowal (1968), Rust (1974), and Pskovskii (1977), indicated that SNe Ia would be precise distance indicators capable of measuring the expansion history of the universe (Phillips 1993). The innovative Calan/Tololo survey (Hamuy et al. 1993), which used photometric plates for discovery and CCDs for follow-up observations, was key to a significant increase in SN discovery. Quickly, pencil-beam surveys designed to discover high-redshift SNe began providing the majority of discoveries (Norgaard-Nielsen et al. 1989; Perlmutter et al. 1997; Schmidt et al. 1998). Rolling searches, where the search epochs and follow-up observations are combined, became an efficient method for observing many transients (Barris et al. 2004), and we still use this strategy today.

In the late 1990s, the Lick Observatory Supernova Search (LOSS; Filippenko 2005) and extremely sophisticated amateur astronomers[24] (e.g., Evans 1994) continued to increase the discovery rate of nearby SNe. Additional scientific discoveries such as the detection of SN progenitor stars in pre-explosion images (e.g., Woosley et al. 1987; Aldering et al. 1994), the connection between SNe and long-duration gamma-ray bursts (Galama et al. 1998; Hjorth et al. 2003; Stanek et al. 2003), and the discovery of the accelerating expansion of the universe (Riess et al. 1998; Perlmutter et al. 1999) made transient discovery even more valuable.

In the past two decades, the discovery rate of astrophysical transients has been increasing at an exponential rate.[25] This is mainly the result of systematic searches for high-redshift SNe (Supernova Cosmology Project, Perlmutter et al. 1997; High-Z Supernova Search, Schmidt et al. 1998; Deep Lens Survey, Becker et al. 2004; Supernova Legacy Survey, Astier et al. 2006; Guy et al. 2010; ESSENCE, Miknaitis et al. 2007; Narayan et al. 2016; SDSS-II, Frieman et al. 2008; Kessler et al. 2009; Sako et al. 2018, Dark Energy Survey, Bernstein et al. 2012; Dark Energy Survey Collaboration et al. 2016; Abbott et al. 2019; Brout et al. 2019a; Pan-STARRS Medium Deep Survey, Rest et al. 2014; Jones et al. 2018b; Villar et al. 2020; HST surveys CANDELS, CLASH, and the Frontier Fields, Graur et al. 2014; Rodney et al. 2014; Kelly et al. 2015, Subaru Hyper Suprime-Cam Transient Survey, Tanaka et al. 2016) and low-redshift SNe (SNFactory, Aldering et al. 2002; Texas Supernova Search, Quimby 2006; SkyMapper, Keller et al. 2007; Scalzo et al. 2017; Catalina Real-Time Transient Survey, Drake et al. 2009; (i) PTF, Law et al. 2009; CHASE, Pignata et al. 2009; MASTER, Lipunov et al. 2010; ATLAS, Tonry 2011; Tonry et al. 2018; La Silla QUEST, Baltay et al. 2013; ASAS-SN, Shappee et al. 2014; PSST, Huber et al. 2015; DLT40, Valenti et al. 2017; ZTF, Bellm et al. 2019b). Recent low-redshift all-sky surveys such as ATLAS, ASAS-SN, and PSST in particular were critical to increasing the transient discovery rate in the past few years, with ZTF now augmenting the rate even further. This recent wealth of time-domain data has led to significant advancement in our understanding of stellar evolution, SN explosion mechanisms, black holes, the chemical enrichment of galaxies, and the fundamental physics of our universe (Campana et al. 2006; Lorimer et al. 2007; Smith et al. 2007; Smartt et al. 2009; Nomoto et al. 2013; Riess et al. 2016; Abbott et al. 2017; Scolnic et al. 2018). In the coming decade, the Vera C. Rubin Observatory will further increase the rate of transient discoveries by *an order of magnitude*, potentially finding 10^5 new transients per year (LSST Science Collaboration et al. 2009).

A number of smaller-scale time-domain surveys are complementing these efforts with multiwavelength and fast-cadence transient searches. Surveys including the Vista Infrared Extragalactic Legacy Survey (Hönig et al. 2017) and the GALEX time-domain survey (Gezari et al. 2013) undertook transient searches in the near-infrared and ultraviolet, respectively. Current fast-cadence searches, including the ZTF one-day survey, DLT40 (Valenti et al. 2017), the Evryscope (Law et al. 2015), the Korea Microlensing Telescope Network (Kim et al. 2016), Kepler (K2; Howell et al. 2014), and TESS (Fausnaugh et al. 2019), have pioneered new techniques to understand transient and variable phenomena on short timescales. However, a number of key questions remain unanswered by current surveys owing to their limited wavelength coverage, area, cadence, depth, or photometric calibration.

Here we describe the Young Supernova Experiment (YSE), a 3 yr survey for transients that focuses on discovering statistical samples of young transients with additional emphasis on discovering rare and red transients, measuring cosmological parameters, and preparing for the Rubin Observatory. YSE began on 2019 November 24 and is currently using 7% of the observing time on Pan-STARRS1 to survey 750 $\deg^2$ of sky with a 3-day cadence to a depth of $gri \approx 21.5$ mag and $z \approx 20.5$ mag; we plan to double the survey area to $\sim$1500 $\deg^2$ in the near future. Our survey strategy emphasizes increased coverage in iz and improved depth to distinguish our transient discovery demographics from other ongoing surveys. It will also leverage the excellent photometric calibration of PS1 for SN Ia cosmology. When possible, we attempt to interleave our observations with those of ZTF for an alternating 1- or 2-day combined cadence, further improving our ability to identify young transients.

Below, in Section 2, we discuss key open questions and challenges in transient astrophysics that can be addressed through a new wide-angle time-domain survey such as YSE—in particular, understanding SN progenitors through observations of young SNe; building a census of faint, fast, and red transients; measuring cosmological parameters; understanding black hole variability and tidal disruption events (TDEs); and preparing for Rubin Observatory science. We will use these goals to motivate the YSE survey strategy in Section 3. YSE vetting and follow-up procedures are described in Section 4,

[24] http://www.rochesterastronomy.org/snimages/lindex.html

[25] SN discovery statistics can be found at https://wis-tns.weizmann.ac.il/stats-maps, at http://www.rochesterastronomy.org/sn2020/snstats.html, and from the Open Supernova Catalog (Guillochon et al. 2017).

and an overview of the YSE survey status and discoveries to date are described in Section 5.

2. YSE Science Drivers: Open Questions and Challenges in Transient Astrophysics

2.1. Young Supernovae

In the hours after a stellar explosion, an SN is still roughly the size of its progenitor star. The shock breakout, which produces a large X-ray and UV photon flux, will "flash ionize" the immediate circumstellar medium (CSM; e.g., Gal-Yam et al. 2014). During this time, the SN shock will also interact with the nearby CSM and any potential companion star, ablating material from its surface. As the ejecta expands, it will smooth out the initial inhomogeneities caused by asymmetric explosions and the initial conditions of the progenitor star.

Flash ionization provides a unique window to examine the CSM before the SN ejecta sweeps it up. If the ionizing spectrum is known and the CSM is optically thin, one can convert measured fluxes from lines of different atomic species into densities and abundances at different radii. Combined with multiwavelength observations (e.g., Chomiuk et al. 2012; Margutti et al. 2012), one can create a holistic picture of the progenitor star's circumstellar environment (Jacobson-Galán et al. 2020a).

Any radioactive elements in the outermost layers of the SN ejecta will also result in additional flux before energy produced in the deeper layers of the ejecta has time to diffuse out. As a result, this can produce "excess" flux relative to the later rising light curve (Piro & Nakar 2013). Excess flux has been seen for several SNe Ia (Marion et al. 2016; Hosseinzadeh et al. 2017; Dimitriadis et al. 2019a; Shappee et al. 2019; Miller et al. 2020) and other peculiar thermonuclear transients (Cao et al. 2015; Jiang et al. 2017), but because of either a limited number of data points or limited color information, the interpretation is often unclear (e.g., Dimitriadis et al. 2019b; Tucker et al. 2019). Earlier detections, higher cadence, additional color information, and early spectroscopy could break such degeneracies.

Luminous mass-loss episodes prior to the SN explosion may also be detectable given a survey with sufficient depth and cadence (Ofek et al. 2014; for a review, see Smith 2014). A particularly spectacular example was a luminous outburst 2 yr before the explosion of the SN Ibn SN 2006jc (Foley et al. 2007; Pastorello et al. 2007). Slightly more common are outbursts likely associated with luminous blue variables (LBVs) before a terminal explosion, such as in SN 2009ip (Smith et al. 2010b; Foley et al. 2011; Pastorello et al. 2013; Margutti et al. 2014) and SN 2015bh (Elias-Rosa et al. 2016; Thöne et al. 2017). Early bumps in the light curves of superluminous SNe (SLSNe) have also been found (e.g., Leloudas et al. 2012; Nicholl et al. 2015, 2017; Smith et al. 2016) and may be due to outbursts prior to the explosion or interaction between the SN and shells of the CSM. A survey with deep time-domain imaging would provide enormous legacy value for analysis of future transients—perhaps discovered even decades later—by enabling deep searches for such outbursts.

2.2. Rare, Faint, Fast, and Red Transients

There is considerable uncertainty in our understanding of the nature of rare classes and subclasses of transients, including peculiar thermonuclear SNe (e.g., SN Iax, SN Ia-CSM, Hamuy et al. 2003; Foley et al. 2013; Ca-rich SNe, Perets et al. 2010; SN 2000cx-like, Li et al. 2001; SN 2002es-like, Ganeshalingam et al. 2010; SN 2006bt-like, Foley et al. 2010; various He-shell explosions, De et al. 2019; Jacobson-Galán et al. 2020b; Miller et al. 2020; Siebert et al. 2020), SLSNe (e.g., Gal-Yam 2012), TDEs (Gezari et al. 2013), low-luminosity transients (e.g., Foley et al. 2009; Valenti et al. 2009; Rodney et al. 2018; Srivastav et al. 2020), fast-evolving blue optical transients (FBOTs; Drout et al. 2014), LBV outbursts (e.g., Van Dyk et al. 2000; Kilpatrick et al. 2018a), and kilonovae (Coulter et al. 2017; Drout et al. 2017; Tanvir et al. 2017).

Transients from many of these classes are rarely discovered because they are intrinsically low luminosity, fast evolving, or red (Siebert et al. 2017). Traditional surveys such as LOSS (Leaman et al. 2011) were designed to detect common SNe and so had cadences of 5–15 days with limiting magnitudes set to detect SNe II in targeted galaxies. These surveys were usually performed with blue-sensitive filters. Such a survey would therefore miss many transients of these uncommon classes even if the intrinsic volumetric rate was high. Surveys such as Gattini-IR (De et al. 2020a), with J-band observations every 2 days and a median limiting mag $J = 15.7$, are just now beginning to explore a redder discovery space. Transients such as intermediate-luminosity red transients (ILRTs; Bond et al. 2009) and luminous red novae (LRN; e.g., Mould et al. 1990; Mason et al. 2010; Nicholls et al. 2013), associated with stellar outbursts and mergers, are some of the faint transient classes that may have been fRequently missed by previous surveys.

Additionally, these small field-of-view (FOV) surveys targeted luminous galaxies to increase their overall discovery yield and rejected potential transients at the centers of galaxies to avoid subtraction false positives and active galactic nucleus (AGN) activity. However, some rare classes occur preferentially in low-luminosity galaxies (Lunnan et al. 2015) and nuclear regions (Bloom et al. 2011), and previous surveys would miss these transients even if they were luminous, blue, and long-lived.

A new, untargeted, red-sensitive survey would not only increase rare transient discoveries from individual epochs but also have the potential to increase discoveries of faint but long-duration transients by stacking multiple search epochs obtained over a period of several nights. This would have a significant impact, for example, on the discovery of gravitationally lensed SNe (glSNe) and SLSNe, where the SNe are luminous and long-lived but their volumetric rates are low. Both classes are predominantly found at high redshift and extend the cosmological eras that can be probed spectroscopically. Red bands are advantageous for glSN discoveries in particular (Wojtak et al. 2019), and systematic detections of glSNe could pave the way for constraining the Hubble constant (H_0) from gravitational time delay measurements (Refsdal 1964). For SLSNe (Knop et al. 1999; Smith et al. 2010a; Quimby et al. 2011), many questions remain about their progenitors, explosion mechanisms, luminosity sources, intrinsic rates, interaction with circumstellar material, and how feedback from these sources affects their host galaxies (Gal-Yam 2019). Surveys capable of discovering SLSNe before peak with high-cadence multiband light curves will enable rapid identification, providing sources for multi-wavelength follow-up and a large statistical sample.

2.3. Cosmology

Perhaps counterintuitively, it is the nearest SN Ia samples that are responsible for most of the systematic uncertainty on measurements of the dark energy equation-of-state parameter, w (Brout et al. 2019b; Jones et al. 2019). Most existing low-z SN Ia observations were compiled on more than 13 different, though partially correlated, photometric systems at a time when cosmological analyses were not yet limited by millimagnitude-level uncertainties. It is critical to replace these legacy data with large, well-calibrated samples of low-z SNe Ia for next-generation cosmological analyses. Large statistical samples of low-z SNe are also ideal for measuring the growth of structure from their peculiar velocities to test general relativity (Howlett et al. 2017; Huterer et al. 2017; Kim et al. 2019; Boruah et al. 2020) and reducing the statistical uncertainty of H_0 (Riess et al. 2016).

The 2020s will have two groundbreaking facilities for measuring cosmological parameters with SNe Ia: the Rubin Observatory and the Roman Space Telescope. However, neither will provide an optimal low-z sample for cosmological parameter measurements. Roman will find few low-z SNe (Hounsell et al. 2018), while the nominal-cadence strategy of Rubin will create large (∼20-day) single-filter gaps in their low-z light curves that would make SN Ia standardization less accurate. Therefore, cosmological measurements with either observatory will likely rely on external low-z data sets. Large, high-cadence, unbiased low-z samples could also be used to refine and extend new models for SN Ia standardization (e.g., Guy et al. 2007; Burns et al. 2011; Saunders et al. 2018; Léget et al. 2020; Mandel et al. 2020), to better constrain relationships between SN Ia distance measurements and host galaxy properties (Rigault et al. 2013, 2020; Jones et al. 2018a; Roman et al. 2018), to improve our understanding of common sources of core-collapse SN (CC SN) contamination in SN Ia cosmology measurements (Jones et al. 2018b; Popovic et al. 2020; Vincenzi et al. 2020), and to increase the number of independent photometric systems on which SNe are observed in order to reduce photometric calibration uncertainties—typically the dominant systematic uncertainty in dark energy measurements.

2.4. Black Hole Variability and TDEs

Varying accretion rates in AGNs and QSOs are reflected in their optical variability. By discovering and monitoring a large number of quasars, it is possible to revisit tests of the damped random walk model of quasar variability (Kelly et al. 2009; MacLeod et al. 2010) and study correlations between quasar variability and physical properties (e.g., Sánchez-Sáez et al. 2018; Kimura et al. 2020). Optical variability is also a useful tool for identifying the relatively elusive AGNs in low-mass galaxies (e.g., Butler & Bloom 2011; Baldassare et al. 2018, 2020; Sánchez-Sáez et al. 2019).

A small fraction of these AGNs and QSOs will evolve dramatically over a period of a few years (MacLeod et al. 2016; Ruan et al. 2016), changing their brightness, the hardness of their spectrum, their ionization state, and the presence of broad spectral lines (LaMassa et al. 2015; Runnoe et al. 2016). Prompt spectroscopic observations immediately after photometric changes are detected may then reveal the underlying physics of these "changing-look quasars" (e.g., MacLeod et al. 2019). By discovering changing-look AGNs in the early stages of their transition, one can monitor the change in black hole accretion physics and the possible buildup of an accretion disk (Gezari et al. 2017).

A survey that can reliably find transients in the cores of galaxies and identify them early also allows TDE discoveries. Detailed multiwavelength follow-up observations of TDEs can trace their full evolution, including the formation of accretion disks (Hung et al. 2020), the formation of jets (Zauderer et al. 2011), and the properties of the black holes themselves (e.g., Auchettl et al. 2017; Hung et al. 2017; Holoien et al. 2019; Mockler et al. 2019; Alexander et al. 2020; van Velzen et al. 2021). Studying the diversity of TDEs constrains the black hole mass function and extends it to lower masses than is possible with AGN observations alone (MacLeod et al. 2012; Kochanek 2016; French et al. 2020). Observations of AGNs or TDEs from *wandering* black holes could constrain their dynamics, a key phase before the formation of black hole binaries, and track the ways in which SMBHs settle to the centers of their host galaxies (Bellovary et al. 2019; Reines et al. 2020).

2.5. Preparation for the Rubin Observatory Era

One of the key transient science challenges of the forthcoming Rubin Observatory era is how to identify unusual or scientifically valuable transients from samples of hundreds of thousands. This could include classifications within the first days or hours of discovery, allowing subsequent spectroscopic or photometric follow-up observations, or full light-curve classifications, necessary for a census of SN rates and luminosity functions, as well as for cosmological parameter measurements with SNe Ia. Recent efforts to classify a diverse sample of transients have been successful (e.g., Boone 2019; Muthukrishna et al. 2019; Villar et al. 2019; Möller & de Boissière 2020), including those that exclusively use contextual host galaxy information (Foley & Mandel 2013; Baldeschi et al. 2020; Gagliano et al. 2020), but the sensitivity of these classifiers to biases and nonrepresentative training samples is often unclear. Training data sets built from existing transient surveys will typically have significantly different photometric filters or cadences than Rubin. Multicolor light curves for thousands of transients within a magnitude-limited but otherwise unbiased discovery space would serve as a vital test bed for training transient brokers and designing efficient follow-up strategies. Light curves with iz coverage in particular are missing from most current time-domain surveys. SNe from the Pan-STARRS Medium Deep Survey will assist with these goals (Hosseinzadeh et al. 2020; Villar et al. 2020), but even that sample lacks examples of several rare classes and rarely has detections within a few days of explosion.

Building a survey that coordinates observations between multiple telescopes would also be useful logistical and conceptual preparation for the Rubin Observatory era, which will pre-announce its pointing plan. This will allow supplemental observations from other telescopes that improve the effective cadence of Rubin.

2.6. Magnitude- and Volume-limited Census of SNe

In spite of thousands of new SN discoveries per year, the rates and luminosity functions of many CC SN classes—especially fainter and redder classes—are highly uncertain (Li et al. 2011b; Perley et al. 2020). This propagates to uncertainty in photometric classification of SNe (Jones et al. 2017), stellar

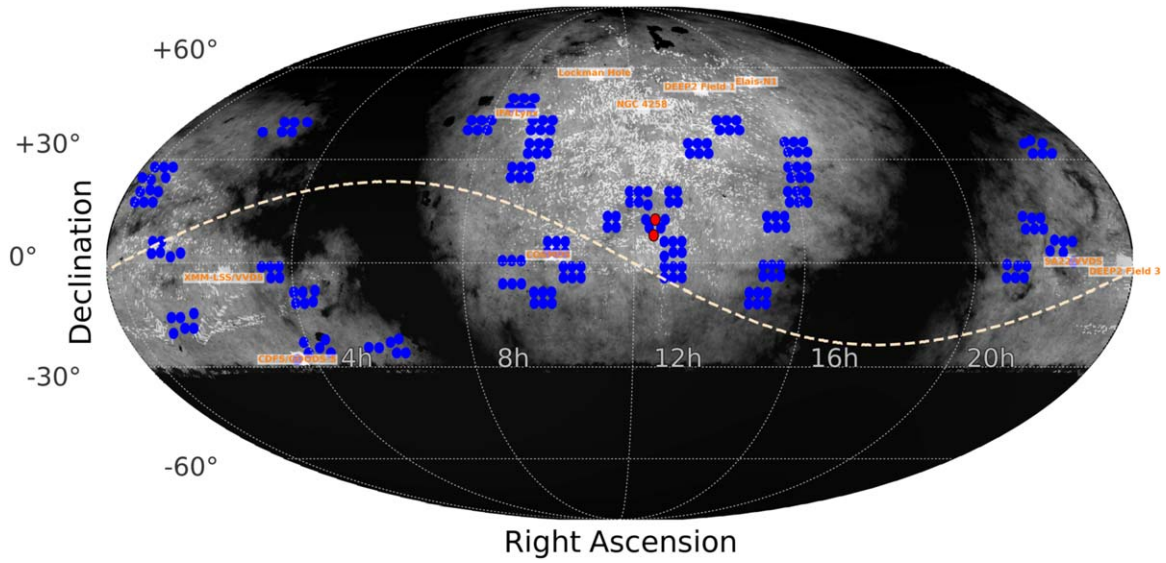

Figure 1. YSE fields chosen prior to 2020 October 1 (blue). The red fields correspond to the two daily Virgo pointings. Lighter (white) background regions correspond to a higher value for the YSE field selection metric (Section 3.3). In addition to this metric, we typically require fields to be at least 20° from the ecliptic plane (dashed line). The labeled high-metric white squares are at the locations of the Pan-STARRS medium deep fields.

evolution, the physics of SN explosions, and the chemical enrichment of the universe (Maoz & Graur 2017). The most often used local rate measurements were measured from a galaxy-targeted survey (Li et al. 2011b), and therefore the rates and luminosity functions are heavily biased by the correlations between SNe and their galaxy environments (Smith et al. 2007; Quimby et al. 2011; Sanders et al. 2012; Taggart & Perley 2019). Blue-sensitive surveys will also not discover highly reddened transients, resulting in a systematic uncertainty for their rate. Since some SNe, particularly those with short-lived progenitor stars, will preferentially occur in dusty environments, the level of bias will be different for each class.

A number of teams, including ASAS-SN (Holoien et al. 2019) and the ZTF Bright Transient Survey (Fremling et al. 2020), are carrying out large surveys to spectroscopically classify all transients within a given magnitude for an improved census of transients that does not rely on galaxy associations, redshift catalogs, and assumed distances. However, a survey with greater sensitivity at redder wavelengths would increase the sample of rare, red SNe that can be discovered, and an extended volume-limited survey, similar to, e.g., De et al. (2020b) from ZTF, would ensure that low-luminosity transients are well represented in the measured rates and luminosity functions. Combining magnitude- and volume-limited surveys leverage the statistics of luminous events in the magnitude-limited sample while preserving the low-luminosity transients in the volume-limited sample. A combined sample would constrain the stellar initial mass function and the progenitor systems of transient classes and subclasses (Strolger et al. 2015).

Table 1
YSE Survey Characteristics

Area[a]	1512 deg^2
Cadence	3 days
Exposure time	27 s
Filter sequence (dark)	*gr*, *gi*
Filter sequence (bright)	*ri*, *rz*
Med. *gri* depth (dark)[b]	21.52, 21.65, 21.37 mag
Med. *riz* depth (bright)[b]	20.87, 20.93, 20.50 mag
Med. FWHM	1.″3
Med. cadence[c]	3.9 days
Pixel scale	0.″25 pix^{-1}
Total area	∼7000 deg^2
griz stack depths[d]	23.6, 23.7, 23.6, 22.8 mag

Notes.
[a] Due to detector masking, YSE will survey ∼1200 deg^2 per epoch, with a variable position angle allowing coverage of the full 1500 deg^2 over a given observing season. Current YSE observations use PS1 only and cover ∼750 deg^2, but we will soon double the area by commencing PS2 observations.
[b] 5σ depths are computed by injecting artificial sources in the nightly YSE images and testing how many are recovered.
[c] Between 2020 March 1 and October 1 to exclude large gaps due to telescope downtime in the first months of the survey. Light-curve gaps due to telescope position angle changes for some transients are not included.
[d] Estimated 5σ depths for 1 yr YSE stacks calculated using the depth computation from Chambers et al. (2016) (see Sections 3.2 and 3.8) and assuming that 30% of epochs are lost owing to weather and 24% are lost owing to detector masking. Over a subset of the YSE area, ∼2000 deg^2, we will reach depths of *griz* ≈ 24.1, 24.3, 24.2, 23.5 mag by combining 3 yr of YSE data. See Table 3 for details.

3. The Young Supernova Experiment: Survey Overview and Strategy

The science goals above motivate the YSE survey design, field selection, and strategy: we wish to design a wide-angle, deep survey with multicolor light curves, including significant coverage at redder wavelengths, and with a survey strategy that facilitates obtaining a statistical sample of young SN detections. Below, we give an overview of the Pan-STARRS telescopes and photometric system, discuss and motivate the YSE survey properties, and use survey simulations to estimate the SN yields from the chosen survey design. YSE fields chosen to date are shown in Figure 1, and basic survey characteristics are given in Table 1.

3.1. Overview of the Pan-STARRS Telescopes, Photometric System, and Data Processing Pipeline

YSE observations use the two 1.8 m Pan-STARRS telescopes (Pan-STARRS1 and Pan-STARRS2), each with 1.4 gigapixel cameras (GPC1 and GPC2; Kaiser et al. 2002). The Pan-STARRS

telescopes have an approximately 7 deg^2 FOV, with that of Pan-STARRS2 (PS2) slightly larger owing to additional CCD chips at the corners of the FOV and the GPC2 detector's reduced masking compared to GPC1. Pan-STARRS1 (PS1) commenced formal survey operation in 2010 May and has currently imaged over 3π sr of the sky (Chambers et al. 2016). PS2 recently finished commissioning. There are subpercent color transformations between the PS1 and PS2 photometric systems.

Pan-STARRS observations are taken through one of six broadband filters, $grizw_{P1}$ (hereafter *grizyw*). The filter transmissions and total system throughput for these filters have been measured via a calibrated photodiode and tunable laser (Tonry et al. 2012). Combined with the well-measured filter functions, the 3π sr of Pan-STARRS sky coverage allowed Schlafly et al. (2012) to solve for the relative calibration of the PS1 photometric system to a precision of better than 5 mmag. Scolnic et al. (2015) then improved the absolute calibration of PS1 by comparing observations of secondary standard stars across multiple photometric systems. The excellent photometric calibration of PS1 is critical for SN cosmology and helpful for many of the other YSE science goals discussed in Section 2.

Pan-STARRS data are processed using the Image Processing Pipeline (IPP) at the University of Hawaii's Institute for Astronomy (Magnier et al. 2020). The IPP is used to download, process, and archive all Pan-STARRS images and includes a difference imaging pipeline to search for transients. Once data are taken and reduced and a template image is convolved and subtracted from the data, the Transient Science Server at Queens University Belfast (Section 4; Smith et al. 2020) uses a combination of massive catalog cross-matching and a machine-learning algorithm to discover transient phenomena in the survey images.

The Pan-STARRS design and infrastructure have enabled a number of innovative transient science programs, notably the Medium Deep Survey (MDS), the Pan-STARRS survey for Transients (PSST; Huber et al. 2015), and recently the Pan-STARRS Search for Kilonovae (McBrien et al. 2021). The Medium Deep Survey observed 70 deg^2 of sky at an average of six observations per 10 days from 2010 to 2014, discovering over 5000 SNe. Approximately 500 of these SNe were classified spectroscopically (Rest et al. 2014; Scolnic et al. 2018), and spectroscopic host galaxy redshifts for over 3000 were obtained (Jones et al. 2017). Science highlights from these data include cosmological parameter measurements (Rest et al. 2014; Jones et al. 2018b), TDE discoveries (Gezari et al. 2013; Chornock et al. 2014), fast-evolving luminous SNe (Drout et al. 2014), SLSNe (Chomiuk et al. 2011; Lunnan et al. 2013; McCrum et al. 2014), SNe Iax (Narayan et al. 2011), and transient classification tools for the Rubin Observatory (Villar et al. 2019).

PSST commenced after the end of the MDS and used the data taken on PS1 through NASA's near-Earth object (NEO) observation program to discover new transients. PSST combines the IPP difference imaging pipeline at the IfA in Hawaii and the Transient Science Server at Queen's University Belfast to search for transients. The PSST team has discovered the majority of the ∼9000 publicly reported PS1 transients. The Pan-STARRS Search for Kilonovae is using these same NEO observations to conduct a volume-limited search for intrinsically faint transients within ∼200 Mpc (McBrien et al. 2021). Though YSE will not carry out LIGO counterpart searches, Pan-STARRS is also a powerful facility for searching for gravitational wave counterparts, due to both the FOV and the existence of reference sky templates for immediate difference images above $\delta \approx -30$. Pan-STARRS has has been employed for this work during the LIGO Scientific Collaboration and Virgo Collaboration's observing runs O1–O3 (e.g., Smartt et al. 2016; Ackley et al. 2020).

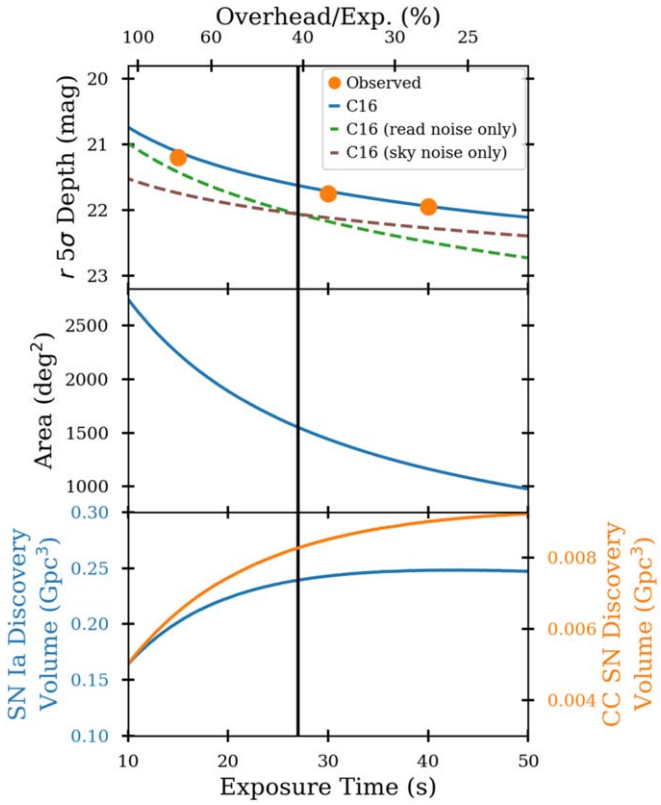

Figure 2. Top: depth as a function of exposure time for PS1 with read noise (green), sky noise (brown), and total noise (blue). Observed depths from the Foundation Supernova Survey at 15, 30, and 40 s are shown in orange, with the overhead (11 s) divided by the exposure time shown on the top axis. Middle: YSE area as a function of exposure time for our fixed total observing time. Bottom: YSE discovery volume for SNe Ia assuming $M_r = -19.3$ mag (blue; left axis) and a nominal CC SN with $M_r = -16.5$ mag (orange; right axis) as a function of exposure time for our fixed total observing time. The black vertical line indicates the chosen YSE exposure time (27 s), which corresponds to the exposure time at which the sky noise begins to dominate in the *r* band.

3.2. Depth, Cadence, Area, and Filters

The Pan-STARRS telescopes allow for a large-area, high-cadence, well-calibrated survey but place a number of constraints on the exposure time and area coverage of YSE. Our team considered only exposure times greater than 15 s; for practical purposes, this is the minimum allowed exposure time to limit systematic uncertainties in the photometry due to the GPC1 shutter. However, the Pan-STARRS cameras also have a relatively high read noise of $8e^-$ (Chambers et al. 2016) and an overhead of approximately 11 s per exposure, which makes it advantageous to increase the YSE exposure time beyond the 15 s minimum.

Figure 2 demonstrates the trade-off between area and volume for different PS1 exposure times. The read noise and sky noise for PS1 during dark time are given by Chambers et al. (2016) and agree with measured depths from Foundation Supernova Survey data (Foley et al. 2018) and PSST. We wish to survey a large volume while still covering a large-enough area to discover many brighter, nearby events and while surveying a

Table 2
Large-area, Extragalactic Transient Surveys

Survey	Area[a]	Cadence	Filters	Mag Lim.[b]	$M = -19$ Volume[c]		$M = -16$ Volume[c]		Pixel Scale	Calib.
					All	Low A_V	All	Low A_V		
	(deg^2)	(days)			(10^{-3} Gpc^3)		(10^{-3} Gpc^3)		(arcsec $pixel^{-1}$)	(mmag)
ATLAS	24,500	2	*co*[d]	$c/o \approx 19.7$	296	230	5.97	4.63	1.86	5
ASAS-SN[e]	20,000	1	*Vg*	$V \approx 17$[f]	7	5	0.13	0.10	8	⋯
PSST[g]	14,000	∼0–15	*iw*	$iw \approx 21, 22$	140	⋯	2.29	⋯	0.25	3
ZTF:										
MSIP[h]	12,975	3	*gr*	$gr = 21.1, 20.9$	850	740	20.22	17.51	1	10
i band	7900	4	*i*	$i = 20.2$	177	⋯	3.75	⋯	1	10
ZTF 1-day	1725	1	*gr*	$gr = 21.1, 20.9$	113	⋯	2.69	⋯	1	10
YSE:										
Full survey	1512	3	*griz*	$gr = 21.5, 21.7$	161	161	4.07	4.07	0.25	3
i band only	1512	6	*i*	$i = 21.4$	135	135	3.35	3.35	0.25	3
z band only	1512	12	*z*	$z = 20.5$[i]	49	49	1.07	1.07	0.25	3
+ZTF MSIP	1512	1.5	*griz*	$gr_{ZTF} = 21.1, 20.9$	70	60	1.59	1.59	⋯	5

Notes. Selected extragalactic transient surveys sorted by area per cadence cycle. Limiting magnitudes and volumes are computed for dark-time observations. Approximate magnitude limits, survey area over the time period of one cadence cycle, and calibration are from Bellm et al. (2019a, 2019b) and Masci et al. (2019) for ZTF, from Schlafly et al. (2012), Scolnic et al. (2015), and this work for YSE, from M. Huber (2021, private communication) for PSST, from Tonry et al. (2018) for ATLAS, and from Holoien et al. (2017) for ASAS-SN. Volume estimates assume flat ΛCDM with $H_0 = 70$ km s^{-1} Mpc^{-1} and $\Omega_m = 0.3$.

[a] Area per cadence cycle.

[b] Dark time, when available.

[c] Using the bluest available band, neglecting MW dust but restricting the volume calculation to $\sim E(B-V) < 0.2$ area in the low-A_V column (Schlafly & Finkbeiner 2011).

[d] "Cyan" and "Orange" bands, combinations of $g + r$ and $r + i$, respectively.

[e] Or ∼30,000 deg^2 every 2–3 days.

[f] Separate dark/bright-time limits were not given by Holoien et al. (2017), with the ASAS-SN website (http://www.astronomy.ohio-state.edu/~assassin/index.shtml) quoting limits down to 18th magnitude.

[g] The PSST cadence is irregular, with ∼1–4 return visits for a given field typically scheduled within 15 days after the initial observation.

[h] The ZTF Phase I survey; the recently begun ZTF Phase II MSIP survey is a 2-day-cadence all-sky survey using 50% of the total telescope time.

[i] Bright-time limit, as YSE does not observe in *z* during dark time.

significant fraction of the ZTF area.[26] Overlap with ZTF enables high-cadence light curves from combined YSE and ZTF data.

After evaluating a number of different strategies (Appendix A), our team chose *griz* exposure times of 27 s. This choice of exposure time satisfies a number of useful criteria. First, YSE observations are ∼0.4–0.8 mag deeper than ZTF, enabling day-before observations—both detections and nondetections—that put useful limits on the ages of newly discovered SNe. Second, while YSE data are read noise dominated in *g* observations taken during dark time, this exposure time ensures that the rest of the data will be background dominated. Finally, a 27 s exposure time nearly maximizes the possible YSE survey volume (Figure 2) but still covers a large area such that more than 100 SNe yr^{-1} will have $r < 18.5$ mag, making them easy to follow spectroscopically using 2 and 3 m class telescopes from the ground.

We considered several different filter sequences for YSE, a number of which are discussed in Appendix A. We decided on a strategy that emphasizes the *iz* filters while also having at least one *g*- or *r*-band observation per epoch, as *gr* observations allow us to measure rise times for young SNe from the combination of YSE and ZTF data without any assumptions on the color of the event. YSE observes in only two filters per night to maximize the survey area while still preserving color information for transient observations. During dark time, we alternate observations of *gr* and *gi*, and in bright time, due to the ∼1 mag lower *g*-band depth, we alternate *ri* and *rz* observations. During brief periods of gray time (moon illumination between 33% and 66%), we alternate *gi* and *gz*.

Finally, YSE observes each field with a 3-day cadence to increase synergy with the ZTF observing strategy and to allow well-sampled light curves for relatively fast-evolving transients.

In Table 2 we compare the YSE survey characteristics with those of other ongoing time-domain surveys. Each of these surveys has unique advantages, with ASAS-SN discovering nearby SNe with extremely fast cadence, ATLAS having a slightly slower cadence compared to ASAS-SN but increased depth and excellent calibration, and ZTF covering less area than ASAS-SN/ATLAS but having greater depth and both high-cadence and *i*-band subsurveys. In terms of area observed at a given time, YSE will observe significantly less area than ASAS-SN, ATLAS, and ZTF. However, YSE's depth is 0.4–0.8 mag deeper than any other survey, and therefore YSE will cover more volume than ASAS-SN, 50%–70% as much volume as ATLAS, depending on the transient luminosity, and ∼20% as much volume as ZTF, with the *i*-band data in particular probing a unique volume equal to 76%–90% of the ZTF *i*-band volume. In terms of the photometric calibration in particular, the excellent PS1 calibration outperforms other systems (and PS2 calibration will be tied to PS1 for comparable accuracy), which is particularly important for SN Ia cosmology.

[26] See also Bellm (2016) for quantitative discussion of the trade-offs between survey volume, area, and cadence for maximizing detection rate of transients and evaluating discovery capabilities of transient surveys.

The oversampled PS1 point-spread function (PSF) may allow for improved image subtraction, which benefits black hole variability and TDE studies by facilitating discoveries near the centers of galaxies. The combined ZTF/YSE cadence is particularly advantageous for fast-cadence studies, helping with discoveries of young SNe, and the z-band coverage is unique to YSE and will aide in the discovery of very red transients.

3.3. Field Selection

We select YSE survey fields based on the following criteria:

1. To increase transient discovery volume, we choose fields with high Galactic latitude and low Milky Way (MW) extinction.
2. We prioritize fields with a large amount of available archival data, primarily redshifts and deep multiwavelength imaging.
3. We prioritize equatorial fields, as they can be observed with follow-up facilities from both hemispheres. However, in most cases we require fields to be at least 20° from the ecliptic plane to minimize observing gaps caused by the Pan-STARRS moon avoidance angle of 30°.
4. We avoid fields with declinations less than −30°, as YSE requires deep template images from previous Pan-STARRS observations, which are scarce at large negative declinations.
5. We choose fields that, given their history of observations, ZTF will typically observe on a 3-day cadence or greater and in two filters.
6. Our observations are interwoven with Pan-STARRS NEO observations, requiring us to space our fields in R.A. so that they can be observed throughout the night.
7. When possible, we place pointings in minimum schedulable blocks of six pointings each, as Pan-STARRS slews of more than 15° require approximately 1 minute of overhead to refocus the telescope.
8. We prioritize new fields with rising or scientifically interesting transients that have been discovered by other time-domain surveys and for which YSE data would be beneficial. We will attempt to follow such transients using as many fields as possible in the first year of the survey and using 50% of fields in subsequent years. The remaining 50% will be kept the same across multiple years for long-term monitoring.
9. We prioritize fields that have a larger number of nearby galaxies within 150 Mpc, with galaxies at <10 Mpc given the highest weight. This will result in a slight bias to the nearby rates in exchange for an increase in SN discoveries, but we expect to be able to correct for this bias in future analyses given the large fraction of galaxies that are untargeted.

We use a semi-arbitrary field selection metric to take these priorities into account, which is discussed in Appendix B. We consider the total amount of HST exposure time when selecting fields, which is important for identifying or constraining progenitor systems in pre-explosion imaging (e.g., Li et al. 2011a; McCully et al. 2014; Foley et al. 2015; Kilpatrick et al. 2018b; Kilpatrick & Foley 2018), as well as the number of active SNe—particularly SNe before maximum light—in a given field, but do not formally include these quantities in the metric. The initial set of YSE pointings is shown in Figure 1.

3.3.1. Daily Survey of Virgo

When the Virgo Cluster is observable at air mass < 1.5, YSE will also dedicate two Pan-STARRS pointings to a daily survey of Virgo. Our team may choose to undertake similar mini-surveys of other nearby clusters, such as Coma, in the future. The Virgo region of the sky produces an extraordinary number of SNe; in the past 15 yr, 30 SNe were spectroscopically classified within the radii of the two YSE Virgo pointings our team has adopted[27] (not accounting for detector masking). Most recently, this includes three SNe Ia (SN 2018bgb, SN 2018axs, and SN 2017eea) and one SN IIn (SN 2017jfs).

YSE will be able to detect pre-explosion outbursts for Virgo transients to an approximate absolute magnitude of −10. We have chosen our pointings to maximize the archival HST exposure time, thereby simultaneously including the majority of Virgo galaxies. A 4 deg^2 deep stack from the first season of observation for our daily M87 Virgo field is shown in Figure 3, along with the locations of six transients observed in the field (five are located in the background of Virgo, and one is in the cluster). These are YSE-observed SN 2020pf (a ZTF discovery but with simultaneous YSE observations) and YSE-discovered SN 2019yub, SN 2020ndg, SN 2020lhy, SN 2020mvx, and finally AT 2020iuy, which is likely a stellar outburst with peak $M_i \approx -11.9$ mag.

3.4. Criteria for Targeted Observations

Although we wish to keep 50% of our fields fixed for long-term monitoring, the other 50% of YSE fields can be adjusted each year to follow new transients that meet our science objectives. We hope to obtain targeted observations of ∼15 SNe per month. This includes rare transients, young transients, or low-z SNe Ia to build an anchor sample for next-generation cosmology surveys. Of these 50% that can be adjusted, our survey requirements specify that 40% of new fields should be within 15° of existing fields to limit refocus overheads. To move an existing YSE survey field to target a new SN, the survey field should meet these criteria (below, a setting field must have air mass greater than 1.5):

1. To relocate an existing field to a new location, the existing field either (a) should have no clearly rising transients and be within 10 days of setting or (b) should have no transients within either 2 weeks of maximum light or within a month of discovery. Certain rising transients that would have very poor light-curve coverage (e.g., if the field is near setting) would also be reasonable candidate fields to move. Conversely, a current field with a post-max SN that is of high scientific value to the collaboration should not be discontinued unless it is near setting.
2. If YSE science will substantially benefit from continued follow-up observations of the transients in the existing field, the field will not be moved.
3. The location of the new field should be within 15° of existing survey fields unless the target is of exceptionally high priority.
4. In most cases, a new field should be 3 months or more from setting.

[27] Using data collected by the Open Supernova Catalog (Guillochon et al. 2017).

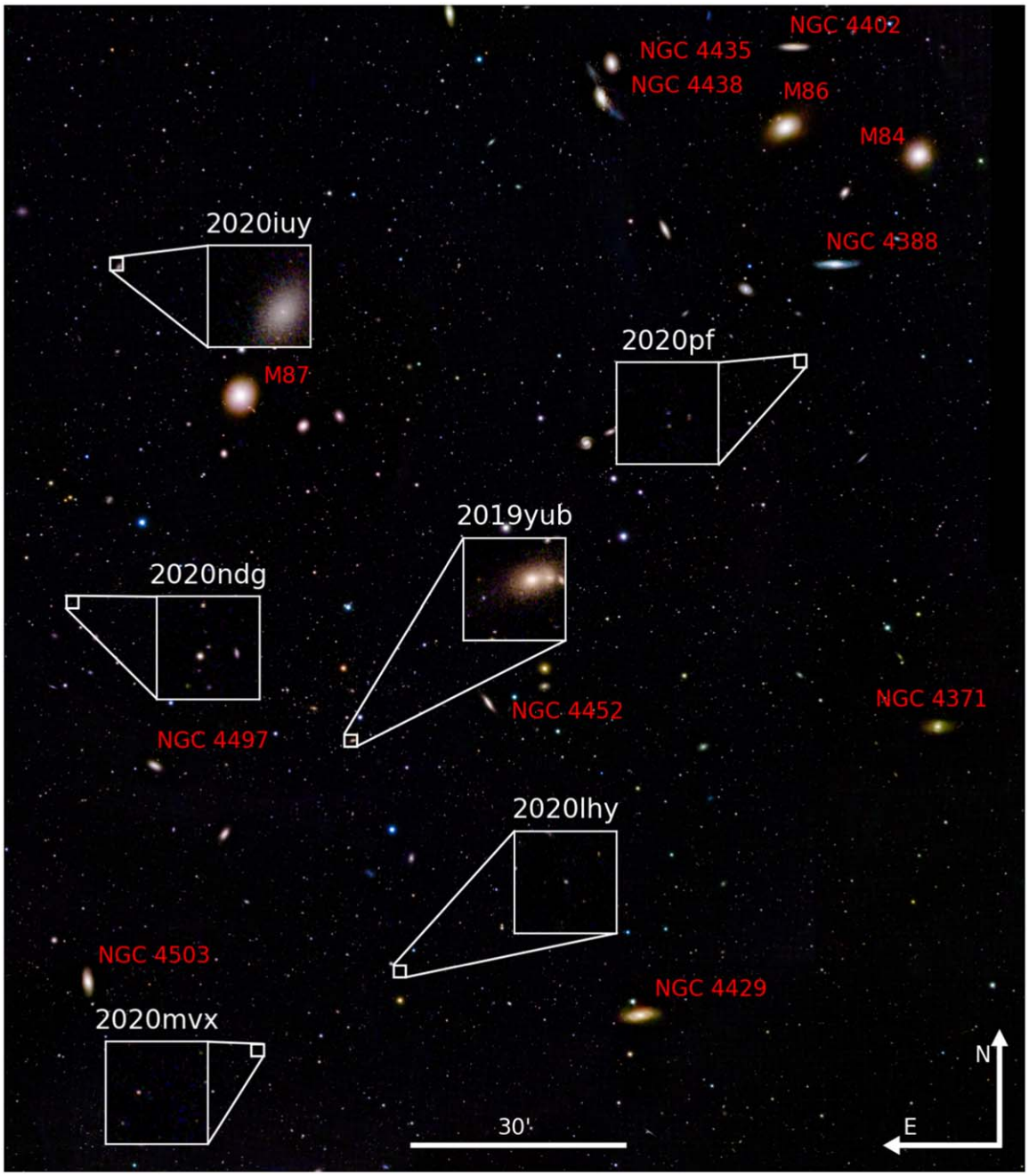

Figure 3. Stacked 2 deg × 2.4 deg image corresponding to part of a YSE daily Virgo Cluster field. A subset of luminous Virgo Cluster galaxies in the field are labeled in red. White boxes show an enlarged view of the host galaxies of transients discovered or observed by YSE in this field, including likely stellar outburst AT 2020iuy at $M_i \approx -12$ mag.

3.5. Interleaving YSE and ZTF Observations

To maximize discoveries of young SNe and increase the effective cadence for many YSE and ZTF transients, we attempt to schedule YSE observations such that they precede ZTF observations by one calendar day. Because our survey is ∼0.4–0.8 mag deeper than ZTF during dark time, we hope to discover fast-rising SNe or newly exploded SNe by observing a >1 mag rise between the Pan-STARRS observation and the ZTF observation approximately 21 hr later. As ZTF reports transient discoveries with a median delay of just ∼10 minutes from the time the image is taken, our team is able to quickly combine the data streams to trigger rapid spectroscopic and multiwavelength follow-up observations of fast-rising SNe.

In practice, predicting ZTF observations can be nontrivial, as ZTF uses a complex scheduling metric to avoid large coverage gaps rather than a fixed 3-day cadence, and weather makes it difficult to anticipate whether an observation will be scheduled or carried out on a given night. However, ZTF generally prioritizes fields by those with the longest time since they were last observed (Bellm et al. 2019b). Over the first 3 months of YSE, during full nights of observing with clear weather at both Haleakala and Palomar, 61% of our observations were taken a day before ZTF observations of the same field (compared to 33% for uncoordinated observations; see Section 5 for examples of our data). However, we find that during longer periods of good weather we are more able to more successfully

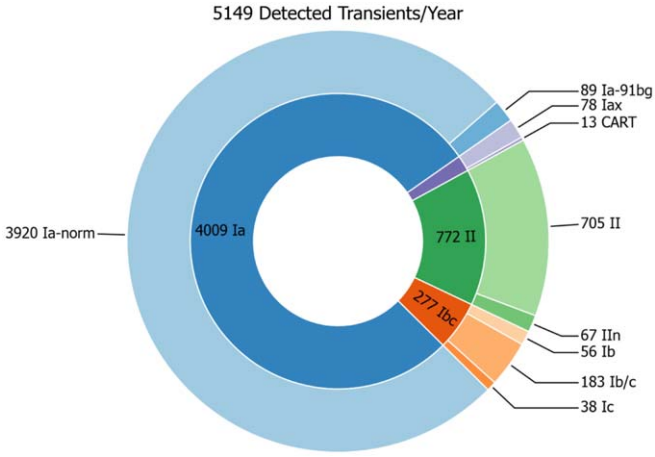

Figure 4. Predicted number of SNe per year with at least three YSE detections of $S/N > 5$, as determined from SNANA simulations. SN models are from PLAsTiCC (Kessler et al. 2019 and references therein). We predict 3920 SNe Ia, 277 SNe Ib/c, 705 SNe II, and 67 SNe IIn each year of full survey operations. We note that PLAsTiCC templates for certain models, including a subset of SNe II and SNe Ib/c, were not given subtypes and thus do not have subtypes here.

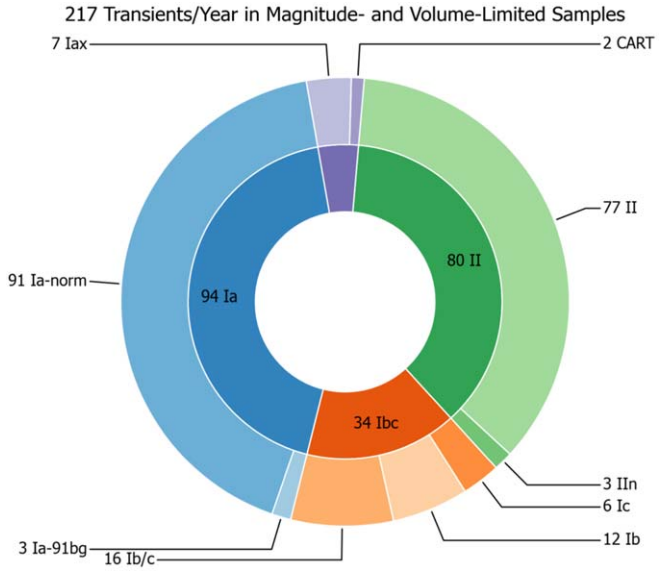

Figure 5. Same as Figure 4, but for YSE SNe per year meeting the criteria of our volume- or magnitude-limited surveys, <250 Mpc or $r < 18.5$ mag (a magnitude at which we expect to be able to obtain spectroscopic classifications). We predict 94 SNe Ia, 34 SNe Ib/c, 77 SNe II, and 3 SNe IIn per year. SN models are from PLAsTiCC (Kessler et al. 2019 and references therein). We note that PLAsTiCC templates for certain models, including a subset of SN II and Ib/c, were not given subtypes. Sixty-one transients (36% of the volume-limited sample) are both more distant than 200 Mpc and fainter than ∼18.5, the limits of the ZTF "Census of the Local Universe" (CLU) and magnitude-limited samples.

predict the ZTF observations. Near the beginning of YSE, most fields were also concentrated within a narrow R.A. window, and these may be less likely to have ZTF observations evenly spread over 3 days. We note that ZTF will soon begin making their nightly observing plans public using the International Virtual Observatory Alliance Observation Locator Table Access Protocol,[28] which will significantly improve our ability to plan overlapping observations. Rubin will also announce their observing schedule via the same protocol, preparing us for potentially allowing YSE to supplement the Rubin cadence in 2023.

3.6. Public Reporting

YSE reports all discoveries of likely transients, omitting likely variable stars or AGNs, to the Transient Name Server[29] (TNS), the official International Astronomical Union mechanism for recording new transient discoveries. Our discovery reports include the first epoch of photometry for each transient (we will provide the first two photometric epochs in the near future), and whenever a team member obtains a spectroscopic classification of an unclassified YSE transient, the spectrum and classification are sent to TNS as well.

Obtaining a second epoch before reporting a discovery is sometimes necessary for asteroid rejection; to avoid substantial ∼1-minute refocusing overheads for Pan-STARRS when slewing more than 15°, our observations in different filters are spaced only ∼4 minutes apart. This makes asteroid rejection more difficult, occasionally necessitating a second observation or confirmation from a second survey in order to confirm that a YSE alert is a bona fide transient. When YSE observations for a new field begin, AGN contamination is also significant; as our team has gained vetting experience, we have become more conservative in promoting candidates during the first epochs of a given field to avoid reporting AGNs. In most cases, however, the colors and presence of nearby host galaxies make transient discoveries unambiguous. In cases where it is unclear whether a transient is a true SN versus an asteroid, variable star, or image artifact, we wait to send these events to TNS until additional epochs of data can clarify whether or not they are bona fide transient phenomena.

3.7. Anticipated SN Yields

To evaluate the effectiveness and expected SN discoveries from the survey strategy presented above, we simulated the YSE survey using the SNANA software (Kessler et al. 2010). We include models of different SN types and subtypes from the PLAsTiCC SN classification challenge (Kessler et al. 2019), including SN Ia, SN Iax, SN II, SN Ib/c, ILOT, and CART. We omit TDEs, SLSNe-I, and kilonovae owing to large uncertainties on their rates, as well as purely theoretical models and nontransient models (e.g., variable stars and AGNs). We use anticipated survey depths from Chambers et al. (2016), moon-phase-dependent sky noise to match 3π observations, SN rates from Strolger et al. (2015) and Dilday et al. (2008), normalization of those rates at $z = 0$ from PLAsTiCC (and references therein; most rates originate from Li et al. 2011b), and a nominal ZTF survey to match their reported depths with ZTF observations scheduled 21 hr after YSE. Details of the simulation methodology and the effect of choosing alternate survey strategies are given in Appendix A.

Summary statistics for the nominal simulated YSE survey design are shown in Figure 4. Due to its depth—YSE is able to find SNe Ia at redshifts up to nearly ∼0.3—simulations predict 5149 SNe per year having at least three detections with a signal-to-noise ratio $(S/N) > 5$, including 3920 SNe Ia, 277 SNe Ib/c, 705 SNe II, and 67 SNe IIn. Our magnitude- and volume- limited samples, comprising SNe with $m < 18.5$ mag and $D < 250$ Mpc, respectively, are expected to contain a total of 217 SNe per year (Figure 5; 49 SNe are members of only the

[28] https://www.ivoa.net/documents/ObsLocTAP/index.html
[29] https://wis-tns.weizmann.ac.il/

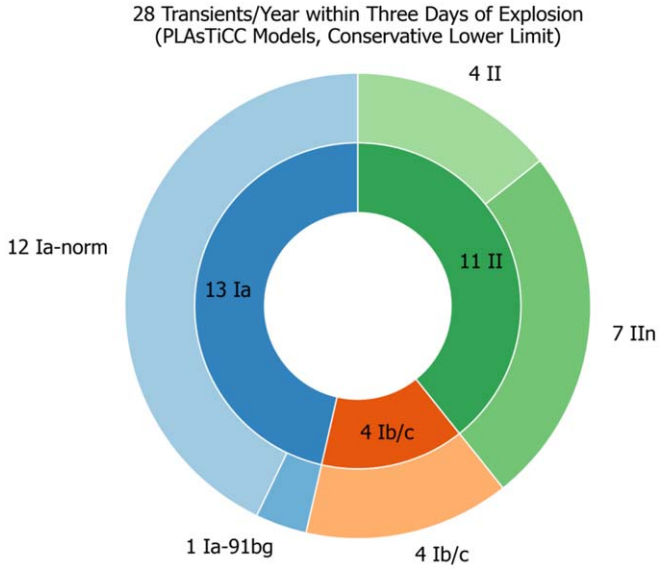

Figure 6. Same as Figure 4, but for YSE SNe per year discovered within 3 days of explosion. Simulations yield 13 SNe Ia, 3 SNe Ib/c, and 11 SNe II. We expect the simulation to underestimate the true number of young SNe since the SALT2 model for SNe Ia has a slower early rise than, for example, the SNe discovered by Jiang et al. (2020), and few PLAsTiCC CC SN models include a shock breakout cooling stage.

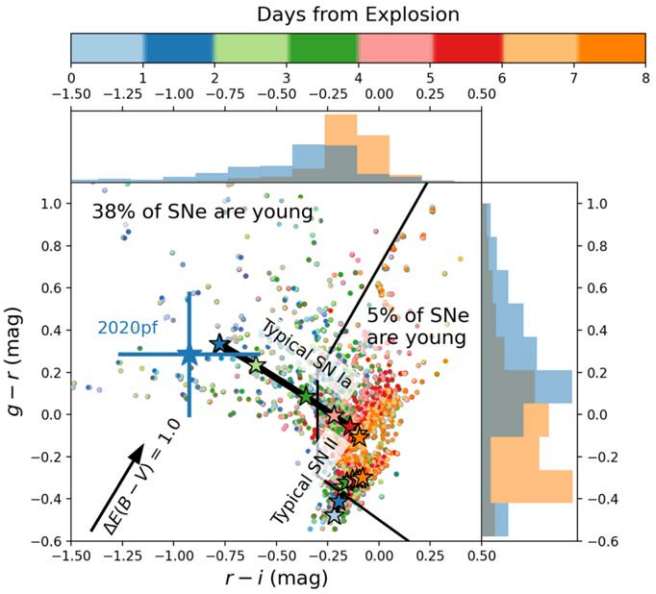

Figure 7. Color–color diagram for "noise-free" YSE SNe as simulated by SNANA, with colored points representing the time since explosion as described by the above color bar. The black arrow indicates the direction and magnitude an object would experience if its dust reddening were increased by 1 mag with $R_V = 3.1$. The black line defines a relatively simple cut that adequately identifies SNe within 3 days of explosion, with 38% of all objects to the left of the line being young, while only 5% of those to the right of the line are young. We highlight the path a typical SN Ia and SN II (star symbols) travel as they evolve from explosion. We note that the $g - r$ and $r - i$ colors are particularly useful for selecting young SNe II and SNe Ia from the entire population, respectively. SN 2020pf at an epoch of ∼2 days after explosion from YSE and ZTF data is displayed as a star with error bars; it is consistent with the simulations and in the defined "early" region. To the top and right are histograms of the $g - r$ and $r - i$ colors for SNe before +3 days from explosion (blue) and after +3 days from explosion (orange).

magnitude-limited survey, 109 are members of only the volume-limited survey, and 59 are members of both).

In Appendix A, we discuss the results of several other survey designs explored by our team, including variations in exposure time, three or four filters per day, and a survey design focused on either blue or red filters. We caution that some simulated yields are affected by small number statistics. As exposure time increases, the number of discovered SNe tends to increase, but begins to flatten after 25 s, as would be expected from Figure 2. Surveys consisting of three or four filters per day would be excellent for some science cases, but would drastically reduce the discovery space for transients, resulting in a 40%–50% reduction in the number of transient discoveries. A blue-focused survey was primarily ruled out because it offers a less unique discovery space compared to existing time-domain surveys, while a survey focusing only on *riz* observations would be expected to reduce young SN yields, as most young SNe are expected to be blue. Our nominal survey design—27 s exposures with a *gr*, *gi* observing sequence during dark time—was settled on as the best choice for YSE, especially given the characteristics of the Pan-STARRS system and our allocated 7% fraction of time on each telescope.

Finally, Figure 6 and Table 5 show the anticipated yields of SNe less than 3 days old assuming that PLAsTiCC models are correct realizations of young SN brightness and color. For example, PLAsTiCC simulations of SNe Ia are based on the SALT2 model, which has a slower rise at early times than observations of SN 2017cbv, SN 2018oh, and a number of SNe discovered by Jiang et al. (2020). Since SNe IIb often show luminous shock breakout cooling (e.g., Richmond et al. 1994; Arcavi et al. 2011; Kilpatrick et al. 2017; Fremling et al. 2019), they are often easy to detect early as well, yet there are no SN IIb templates in the PLAsTiCC set. It is therefore difficult to truly predict the number of young SNe that will be discovered by YSE, but we note that our team has already observed a handful of young SN candidates, including SNe Ia SN 2020pf, SN 2020fci, SN 2020ioz, SN 2020juq, and SN 2020nbo and CC SNe SN 2020pni, SN 2020kpz, and SN 2020tlf, that are almost certainly within 3 days of explosion or less (see Section 5).

Figure 7 also shows the simulated colors of young SNe; we find that a simple color cut could identify a subset of young SNe with ∼40% accuracy, which is a reasonably high confidence given the follow-up resources available. We find that $g - r$ colors are useful for separating young versus old CC SNe and YSE $r - i$ colors appear to be excellent indicators of young SNe Ia, complementing $g - r$ observations from YSE and ZTF. Our team is working on more sophisticated classification methods using existing observations of young SNe.

While these simulations are state of the art for transient survey planning, they still lack several details for precise estimates. Although early YSE survey yields are returning the expected number of volume- and magnitude-limited SNe, just 26% of transients to date are above the median predicted survey redshift of 0.19. This is likely because our algorithm for measuring YSE photometry has been obtaining inflated uncertainties, effectively reducing the S/N of YSE photometry and our detection efficiency. We identified this issue by implementing a second photometric reduction algorithm and are currently working to implement a fix to our pipeline photometry. Other contributing factors may include biases in the photo-z determinations, as reliable redshifts are more difficult to estimate for faint or undetected host galaxies. Additional stacked observations may

also reduce the noise in the template images, which simulations assume to be negligible. Finally, efficiency losses in the machine-learning "real/bogus" algorithm (Section 4) may also reduce the number of discovered SNe as a function of S/N. Nevertheless, we have observed or discovered 916 transients over the first 10 months of the survey while observing at half of our nominal area and experiencing ∼2 months of downtime.

3.8. Impact on YSE Science Drivers

Given the YSE survey design and simulations described above, we briefly summarize a number of ways in which the YSE data will address the science drivers identified in Section 2:

1. Young SNe. YSE will discover at least two SNe within 3 days of explosion per month, with a larger sample likely due to known deficiencies in the PLAsTiCC models used to generate YSE simulations. Many of these SNe will have i or z photometry at very early times and can be discovered by YSE ∼ 1 day before they are found by other surveys. Several examples from early YSE data are discussed in Section 5.
2. Red and Rare Transients. The iz coverage of YSE will aid the identification of very red transients. YSE's additional ∼1.2 mag i-band depth compared to ZTF will probe a unique volume equal to ∼76%–90% of the ZTF i-band survey volume (Table 2). YSE is also the only time-domain survey currently observing in the z band. Within our volume-limited sample out to 250 Mpc, we will discover transients down to $M_i \approx -15.5$ mag and $M_z \approx -16.5$ mag. We also expect YSE to observe two glSNe per year in regular sky scans and up to five glSNe per year in stacked images based on projections from Wojtak et al. (2019). YSE fields to date include ∼1400 galaxies near enough for YSE to discover luminous red novae, though their volumetric rate is not well known (Pastorello et al. 2019).
3. Cosmology. The YSE SN Ia sample will be a mix of targeted SN Ia observations to increase the $z \lesssim 0.05$ sample size, using a strategy modeled after the Foundation Supernova Survey (Foley et al. 2018), and untargeted observations, which will have a median redshift of $z \approx 0.12$ (Appendix A). The untargeted sample will include up to 350 $z < 0.1$ SNe per year with a well-understood, magnitude-limited selection and lower uncertainties from peculiar velocities than other low-z samples. The large sample with $z > 0.1$ will serve as an important sample for measuring w, testing general relativity, and helping to understand CC SN contamination in future cosmology analyses. The photometric calibration of the sample will be more precise than any non-Pan-STARRS low-z sample.
4. Black Holes and TDEs. We did not include TDEs in survey simulations, as their redshift-dependent rates are uncertain, as is the efficiency of detecting them in the bright cores of galaxies; based on the survey magnitude limit alone with the rates and luminosities from van Velzen et al. (2021), and including an approximate mean $M_g = -17.5$ mag, we would expect ∼20 per year—and YSE has already observed two TDEs in untargeted observations just in early survey data (a third, AT 2020nov, was targeted; Section 5)—but due to the difficulty of detecting transients in the cores of galaxies, it is unclear whether the expected number from these order-of-magnitude estimates is overly optimistic. YSE survey data will also contain tens of thousands of AGNs for variability studies, and its oversampled PSF may make it easier to detect transients at the bright cores of galaxies compared to other low-z surveys.
5. Preparation for the Rubin Observatory. YSE will measure $griz$ light curves for hundreds of spectroscopically classified transients and thousands of transients in total, including hundreds of detections within the first few days of explosion. This will allow YSE to serve as a unique and invaluable training sample for the Rubin Observatory, adding fidelity to early-time and full light-curve classifications and constraining the rates of rare classes that will exist in Rubin survey data.
6. Magnitude- and Volume-limited Census of SNe. The iz coverage of YSE will improve the census of red transients, and the YSE redshift range will allow a longer lever arm on the redshift-dependent rates of many transients compared to other ongoing surveys. We plan to spectroscopically classify every SN that is either brighter than $r \approx 18.5$ mag at peak or nearer than 250 Mpc, a sample of ≈217 SNe per year (Section 3.7) to constrain both the rates and luminosity functions of SN types and subtypes. Approximately 61 of these SNe (36% of the volume-limited sample and 28% of the total) will be both fainter than $r \approx 18.5$ and more distant than 200 Mpc, the limits of the ZTF magnitude-limited and CLU samples. Additionally, we include photometric redshift estimates in building our volume-limited sample in order to avoid completeness limitations that affect spectroscopic catalogs of the local volume (and the CLU sample to some degree).

Table 3
Stacked Image Depths

Survey	Area (deg^2)	Depth g (mag)	r (mag)	i (mag)	z (mag)
PS1 3π	30000	23.3	23.2	23.1	22.3
SDSS	15044	23.3	23.1	22.3	20.8
DES DR1[a]	5186	24.3	24.1	23.4	22.7
KiDS DR4	1006	25.1	25.0	23.7	
YSE+3π 1 yr	∼5000	23.6	23.7	23.6	22.8
YSE+3π 3 yr (deep[b])	∼2000	24.0	24.2	24.1	23.3
YSE+3π 3 yr (wide[c])	∼7000	23.6	23.7	23.6	22.8

Notes. YSE projected stacked image depths compared to several large-area surveys with observations in the $griz$ bands. Limits for SDSS, PS1 3π, DES, and the Kilo-Degree Survey (KiDS) are from York et al. (2000), Chambers et al. (2016), Abbott et al. (2018), and Kuijken et al. (2019), respectively.
[a] 10σ limits.
[b] Corresponding to the region monitored for the entire 3 yr.
[c] Corresponding to the region monitored for 1–2 yr.

In addition to addressing these time-domain science questions, YSE will create 1 yr stacked images over approximately 7000 deg^2 of sky and 3 yr stacked images over an additional ∼2000 deg^2 of sky. Using the typical read-noise and moon-dependent sky-noise values from Chambers et al. (2016) and assuming 30% loss due to weather and 24% due to pixel masking, we roughly estimate that in 1 yr stacks YSE+3π will reach depths of $griz \approx 23.6, 23.7, 23.6, 22.8$ mag. In the 3 yr stacks YSE+3π will reach depths of $griz \approx 24.0, 24.2, 24.1, 23.3$ mag. Comparisons to the depths of several other large-area surveys are shown in Table 3.

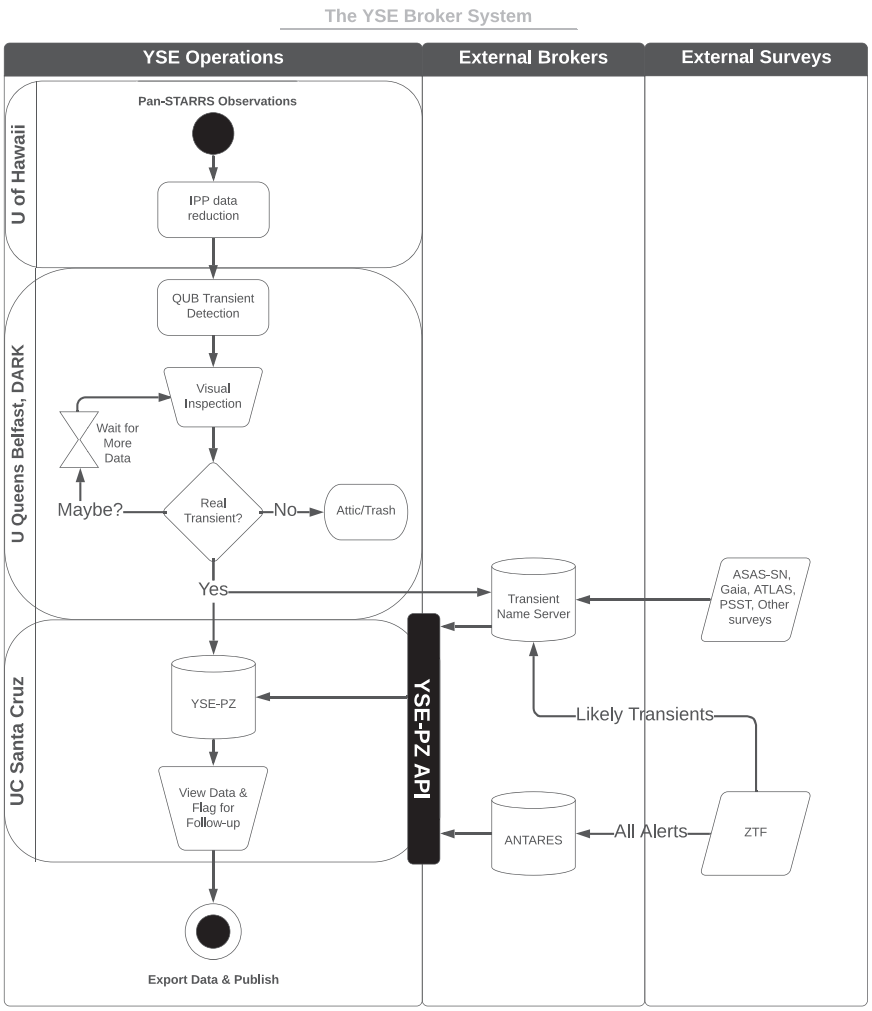

Figure 8. Activity diagram for the YSE Transient Broker process as described in Section 4. The left column indicates the progress and locations of the data and metadata. Data are reduced in Hawaii and sent to the Transient Science Server at Queens University Belfast; members of our team at DARK (U. Copenhagen) visually inspect each event that passes machine-learning cuts. Real transients are reported to TNS, likely AGNs or asteroids are given "attic" designations, and image artifacts are sent to "garbage." Finally, YSE data are combined with public data from other surveys, at which point our team sorts the discoveries and requests follow-up observations of interesting transients. In addition to the workflow shown here, YSE-PZ can request forced photometry upper limits directly from the IPP for new ANTARES or TNS transients without Pan-STARRS detections.

4. Vetting and Following Transients

Efficiently working with large time-domain data sets to identify transients of interest for follow-up observations and facilitating large statistical analyses with the data are key challenges of transient discovery searches (Bloom et al. 2012; Kasliwal et al. 2019; van der Walt et al. 2019). Efficiently separating data artifacts from bona fide transients (e.g., Duev et al. 2019) is also critical. YSE in particular requires a robust and efficient broker process for discovering and following transients.

Once YSE data are taken, they are first processed by the IPP difference image pipeline and sent to the Transient Science Server at Queens University Belfast (Smith et al. 2020). The Transient Science Server then determines the likelihood that each SN is a bona fide transient, including a visual inspection stage performed by our team. From there, possible transients are sent to a transient database and web application housed at UC Santa Cruz, which we refer to as "YSE-PZ." The full YSE broker process is summarized in Figure 8, and the details of this process are discussed below.

4.1. The Transient Science Server

The Transient Science Server removes YSE detections from known AGNs, variable stars, and moving objects using a library of catalogs (see Smith et al. 2020 for details) and employs both pixel-based and catalog-based machine-learning algorithms—i.e., the algorithm is based on both the pixels themselves and photometric metadata such as PSF shape—to remove likely image artifacts and assign a "real-bogus" score to each detection. Candidates are included on the by-eye vetting list if the real-bogus score considers them to be real with at least 32% confidence; we choose this threshold because the training procedure estimates that it will yield a high fraction of real candidates (75%), while rejecting just 1% of bona fide transients. We require 3.5σ detections in at least two separate images (possibly over multiple epochs) to add a source to the list of candidates to be vetted. The machine-learning algorithm is trained using slow-moving asteroids as the "good" objects; we plan to retrain using real transients in more realistic host galaxy environments in the future. Additional details of the algorithm are given in Smith et al. (2020).

If members of our team determine that a candidate is likely a bona fide transient, they are immediately sent to the TNS along with the first epoch of photometric data. If we are unsure, the transients remain on a "possible" list until more data have been collected. Both the transients on the "good" and "possible" lists are ingested to YSE-PZ for combining with data from other surveys and making follow-up decisions.

4.2. YSE-PZ: The YSE Transient Management System

The YSE-PZ application (YSE-PrioritiZe) is designed to ingest every transient reported to the TNS (see footnote 29) to facilitate queries of the data, combine YSE transients with external data, store follow-up data obtained by our team, and enable easy communication among team members for vetting and following new transients. YSE-PZ is a Django-based application built on a MySQL database. The code base is publicly available at https://github.com/davecoulter/YSE_PZ, and we encourage collaboration and new contributors. An example of the web application interface is shown in Figure 9.

YSE-PZ will be described in detail in D. A. Coulter et al. (2021, in preparation). Here, we summarize key features that allow our team to prioritize and organize follow-up observations of transients:

1. Data ingestion from ZTF and TNS. We ingest ZTF alerts using the ANTARES broker (Narayan et al. 2018) for events in our survey fields that have not yet been reported to TNS. We also ingest every transient reported to TNS using the TNS API. For transients that have been reported to TNS, we ingest ZTF photometry from MARS.[30]
2. Dashboard and Initial Transient Vetting. Transients are ingested into YSE-PZ with a status of "New" and then parsed into categories of "Watch," "Interesting," "FollowupRequested," "Following," or "Ignore" based on characteristics such as brightness, redshift, classification, or color. Transients that meet the YSE volume- or magnitude-limited survey criteria are prioritized for follow-up by moving them to "Interesting" or "FollowupRequested," and subsequent queries are used to flag transients that brighten to the point where they are included in the magnitude-limited criteria. YSE-PZ compiles a large amount of data and metadata to aid in the vetting process, including survey images, archival images, other external data (e.g., HST or Chandra imaging), MW extinction, photometry, spectra, classifications, and discovery details. Our team sorts through new transient discoveries daily.
3. Follow-up Requests. YSE-PZ allows follow-up observations to be requested on any telescope for which our team has access. Follow-up requests are added to a custom page for a given observing night and resource, where observers can prioritize the requests and schedule observations. Finder charts using Pan-STARRS 3π imaging may be generated through the web interface, and we plan to add additional tools to facilitate scheduling in the near future.
4. Queries. YSE-PZ allows users to query on any field in the database. A query, once completed and saved, can be added to a user's personal "dashboard" to allow each user to be alerted to transients that are relevant to their science interests. Example queries include the YSE volume-limited sample of transients within 250 Mpc, or transients rising by more than 0.5 mag in a day in a given filter. As new transients are ingested, users can choose to be alerted via email or text message to transients that match a given query to enable extremely rapid follow-up observations.

YSE-PZ is under active development, and new features are continually being added. A well-developed, open-source, robust transient management framework is vital to our science goals and a key part of developing tools for the next decade of transient science.

5. Survey Status and Discoveries to Date

YSE has discovered or observed a total of 8.3% of IAU-reported 2020 transients within our survey fields. YSE has announced a total of 778 discoveries as of 2020 October 1. Though early discovery announcements included significant AGN contamination, our team has become much more accurate over time at removing AGNs, asteroids, and artifacts (burns, persistence, etc.) that passed initial cuts; after inspecting the full YSE light curves to remove these objects, we estimate that YSE discovered or observed 916 bona fide transients prior to 2020 October 1. A summary of our discovery and follow-up statistics is reported in Table 4, and sample light curves are shown in Figure 10. Magnitude and redshift histograms for YSE transients to date are shown in Figure 11.

To date, YSE observations have a median PSF FWHM of $1\farcs3$ and 5σ detection limits of $gri \approx 21.5$, 21.7, and 21.4 mag during dark time and $riz \approx 20.9$, 20.9, and 20.5 mag during bright time (Table 1). After weather loss, we observe with a median cadence of 3.9 days. The median phase of the first $S/N > 3$ observation for YSE transients (based on estimates of the time of maximum light) is -6.4 days.[31]

YSE observations include 138 spectroscopically classified transients (Figure 12); highlights include two SNe Iax (SN 2020inp and SN 2020sck), one super-Chandrasekhar SN Ia (SN 2020esm), four SNe IIb (SN 2020fqv, SN 2020ikq, SN 2020ivg, SN 2020tkc), one SN Ic-BL (SN 2020fhj), and three TDEs (AT 2020neh, AT 2020nov, and AT 2020opy), with AT 2020neh being particularly unusual in its rapid evolution.[32] We have observed several SNe Ia within 2–3 days of explosion, including SN 2020fci, SN 2020ioz, SN 2020juq, SN 2020nbo, and SN 2020pf, among other candidates. We also observed flash ionization features in Keck spectra of CC SNe SN 2020pni and SN 2020tlf, and for SN 2020pni we observed a strong UV peak in Swift photometry at approximately 1.9 days after explosion thanks to ZTF detections within 1 day of explosion and deep YSE nondetections 2 days prior (Figure 13). The early rise of SN Ia SN 2020pf is shown in Figure 14, with the first detection occurring at approximately 19 days before B-band maximum light as determined from a fit of the light curve using SALT2.

We have obtained targeted YSE survey observations of nearby stripped-envelope SNe SN 2019yvr (Ib), SN 2020oi

[30] http://Mars.lco.global/

[31] This phase is roughly equivalent to the discovery epoch, but our discovery reports are sometimes delayed as discussed in Section 3.6.

[32] See Astronomer's Telegrams and AstroNotes from YSE team members for SN 2020tlf and SN 2020tkc (Dimitriadis et al. 2020b), SN 2020fhj (Izzo et al. 2020), SN 2020inp (Dimitriadis et al. 2020a), and AT 2020neh (Angus et al. 2020).

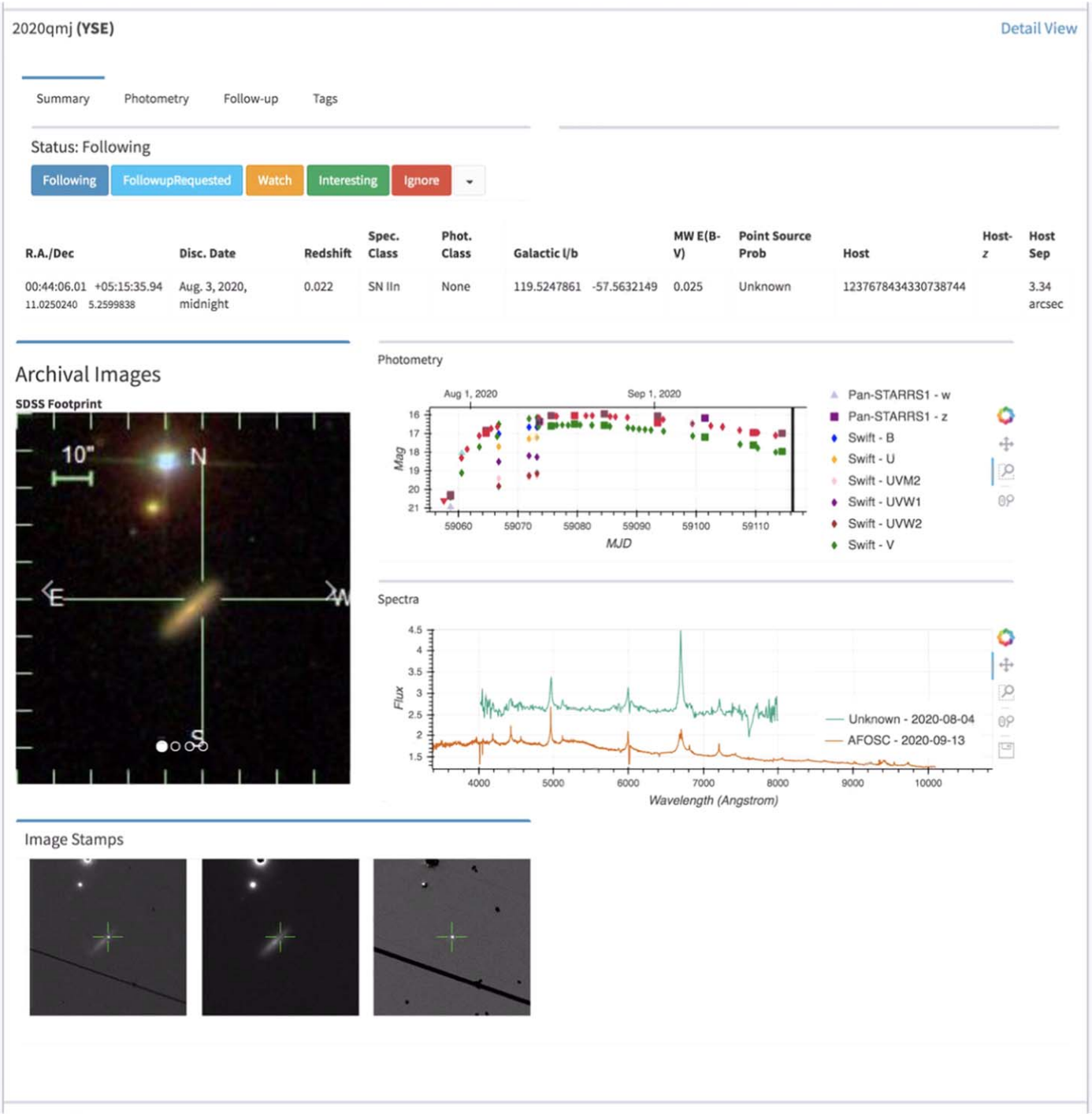

Figure 9. Example "transient summary" page from the YSE-PZ web application. Transient summary pages show YSE image stamps, spectra, photometry, archival images, and metadata, with a more extensive set of data and metadata available via the "detail view."

(Ic), and SN 2020nxt (Ibn), as well as four very nearby SNe Ia, SN 2020jgl and SN 2020uxz and Virgo-adjacent SN 2020ue and SN 2020nlb; analyses of these exciting objects are forthcoming. SN 2020ees, SN 2020fqv, and SN 2020nxt have contemporaneous HST observations, while an additional 10 YSE transients have HST pre-explosion imaging. We are working with ongoing programs such as "Supernovae in the near-Infrared avec Hubble" (SIRAH; HST-GO 15889, PI: Saurabh Jha) to share promising young SNe for coordinated observations with HST and other facilities. We welcome external collaborators; our external scientist policy, together with a guide to the application, can be found at https://yse.ucsc.edu/collaborate/.

Given telescope downtime, we have effectively observed ∼7 months to date, which equates to approximately 3.5 months of the survey simulations in Section 3.7, as they assume double the area coverage. By this estimation we are slightly underperforming our expected yields of ∼5000 SNe per year, but this

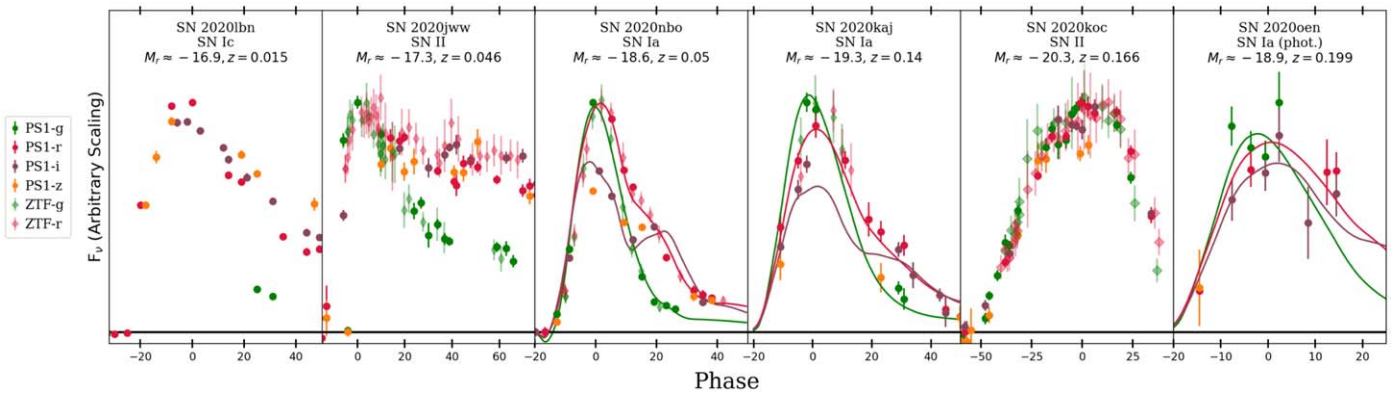

Figure 10. Examples of YSE SN light curves by increasing redshift, from $z = 0.02$ to $z = 0.2$. For the SNe Ia, we also display the best-fit SALT2.4 template light curves (Guy et al. 2010; Betoule et al. 2014) for illustration. ZTF *gr* light curves are displayed as lightly shaded diamonds when available, which effectively doubles the cadence of nearby SNe in our sample (though low-z SN Ic 2020lbn, left, has no public ZTF data). We note that CC SNe SN 2020hrw and SN 2020koc are somewhat unusual SNe, as SN 2020hrw is likely an SN 1987A-like SN and SN 2020koc is unusually luminous for an SN II (although perhaps not quite luminous enough to be considered an SLSN).

Table 4
Initial Statistics of SNe Observed by YSE

	$N_{\rm transients}$
All SNe[a]	916
Discovered by YSE[a]	363
Spec.-confirmed SNe	138
$r \lesssim 18.5$	125
$D \lesssim 250$ Mpc	180
SNe Ia with phase < -10 days	30

Notes. Transient discovery statistics between 2019 November 24 and 2020 October 1. We have been at 50% of our full observing allocation since early January, but we lost ∼2 months owing to weather and telescope malfunctions.
[a] Excluding candidate transients deemed later to be likely variable sources such as AGNs.

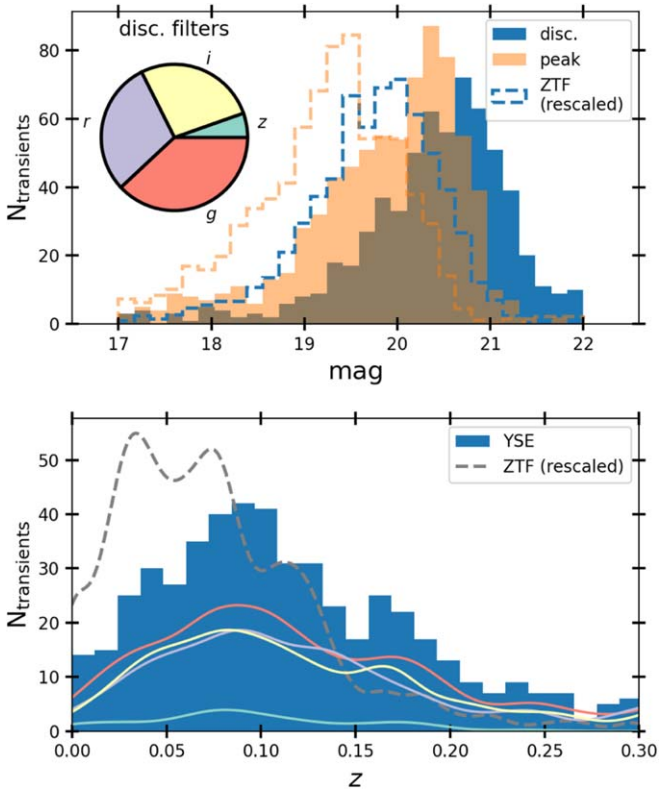

Figure 11. Top: approximate peak and discovery magnitudes for YSE transients to date, including targeted follow-up observations, with the filter combinations used at each discovery epoch or first observation shown in the pie chart. Histograms of 2020 ZTF discoveries, rescaled to match the total number of YSE discoveries, are shown with dashed lines. Estimated peak magnitudes are taken from the brightest epoch, regardless of filter, and include publicly reported observations when available. Discovery magnitudes are more often from the bluer of the two filters at the discovery epoch, as the bluer observation is typically performed first. Bottom: redshift distribution (using an internal photo-z estimate trained on SDSS data, when necessary) for the YSE sample to date. The normalized ZTF redshift histogram for 2020 discoveries to date is shown in gray. Lines show Gaussian kernel density estimates for discoveries in each filter, with colors corresponding to the pie chart in the top panel. Photo-z outliers may artificially increase the numbers in some high-redshift bins.

is expected, as early survey photometry has overestimated photometric uncertainties by factors of 1.7–1.9 (see Section 3.7). Our current magnitude-limited sample of 125 SNe is much larger than expected from the 108 predicted SNe per year in our simulations, though a handful of targeted SNe and survey edge effects as we catch slow-declining SNe when we begin observations of new fields have likely boosted this number significantly. Our volume-limited sample also exceeds that expected from simulations, though this number may also be impacted by photo-z uncertainties.

Our team aims to obtain a spectrum of every unclassified transient with peak $r < 18.5$ mag, $D < 250$ Mpc, or a detection within 2 days of explosion for an estimated total of 217 per year (Figure 5). Our sample will necessarily include classifications by the community, and we are grateful to the teams responsible for helping to classify transients in the YSE magnitude- and volume-limited samples. To date, there have been significant contributions to classifications in this sample from ZTF, ePESSTO+ (Smartt et al. 2015), and the SIRAH team. Our secondary priority will be to spectroscopically classify transients that appear unusual based on their photometric properties.

Our current magnitude-limited sample is 91% spectroscopically complete. We examined the failures, and the two most common reasons for a lack of a spectrum are lack of spectroscopic resources because of COVID-19 shutdowns and the transient being discovered shortly before it sets. Therefore, we are optimistic that our completeness can increase as the survey continues.

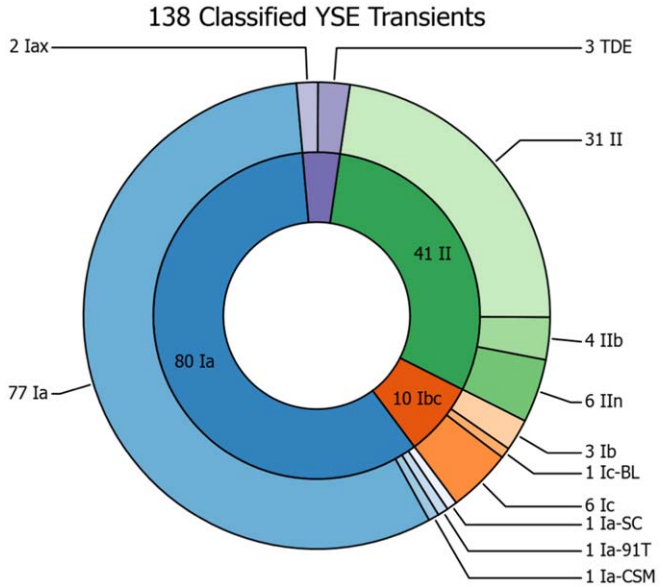

Figure 12. To-date, by-type breakdown of the 138 spectroscopically classified YSE SNe prior to 2020 October 1.

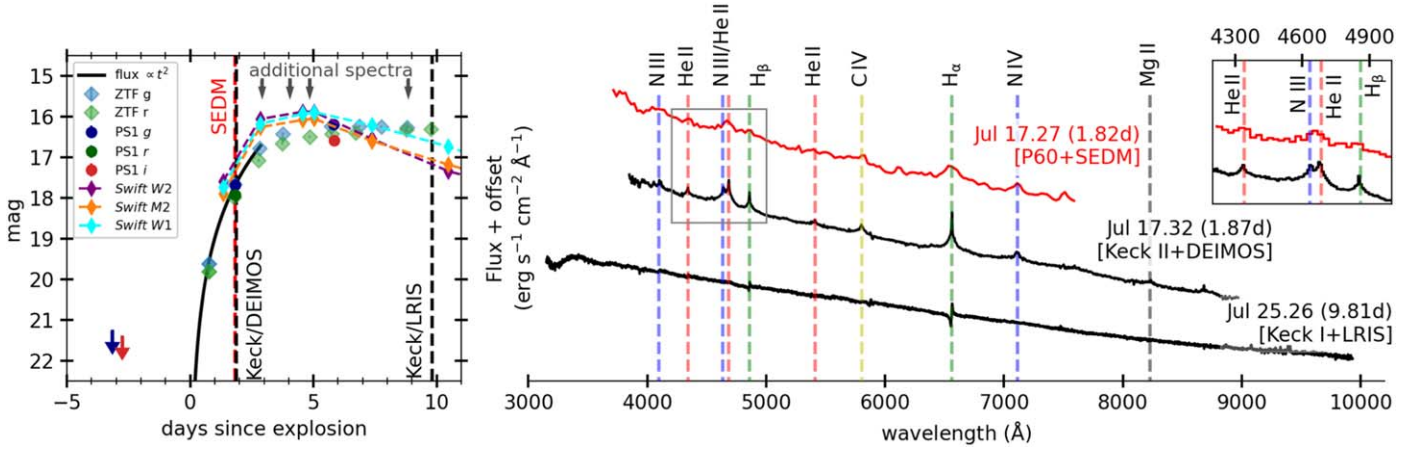

Figure 13. Early light curve (left) and spectra (right) for CC SN 2020pni. ZTF detected SN 2020pni approximately 0.8 days after explosion (Forster et al. 2020), with deep YSE nondetections (arrows; data are taken ∼4 minutes apart but are horizontally spaced for visual clarity) coming 2 days prior. Swift follow-up observations were triggered, and Palomar 60-inch (Bruch et al. 2020a, 2020b) and Keck spectra showing the flash-ionized CSM were taken, all within 2 days of explosion. Flash ionization features had disappeared by approximately 5 days after explosion. Our full analysis will be presented in G. Terreran et al. (2021, in preparation).

6. Conclusions

YSE is a transient survey that will use 7% of the time on both the Pan-STARRS1 and Pan-STARRS2 telescopes to survey 1512 deg^2 in *griz* with a 3-day cadence and two filters per epoch. YSE began on 2019 November 24 and has been running for the past several months using only Pan-STARRS1 but will soon double its observing time by using Pan-STARRS2. Detailed simulations indicate that at full capacity YSE will discover ∼5000 SNe per year. YSE images reach limiting magnitudes of ∼21.5 in *gri* and ∼20.5 in *z*, with dark- and bright-time observations taken in combinations of *gri* and *riz*, respectively. The YSE survey strategy avoids the Galactic plane and prioritizes equatorial fields with a high volume of archival and, when possible, multiwavelength data. YSE is currently planning to carry out a 3 yr survey; survey updates and contact information for members of our team can be found at https://yse.ucsc.edu. Given that we have not yet begun surveying the full YSE area, we are optimistic that YSE will continue through the anticipated start of operations at Rubin Observatory in 2023.

The primary science drivers of YSE include opening a new discovery space for faint and red transients, building a census of transients in the nearby universe, understanding black hole variability and TDEs, and assembling a legacy high-cadence, low-*z* SN Ia cosmology sample to complement high-redshift samples from the Rubin Observatory and the Roman Space Telescope. YSE has discovered or observed 916 SNe to date and 8.3% of the likely transients announced so far in 2020.

When Pan-STARRS2 observations commence, we anticipate that the YSE survey volume will be ∼20% that of ZTF and the *i*-band volume will be ∼75%–90% that of ZTF (Table 2; estimates depend on the luminosity of the transient). We will have YSE data for approximately 10% of ZTF transients in the public survey, giving thousands of light curves with combined observations every 1–2 days. We will also have a sample of thousands of cosmologically useful SNe Ia with ∼3 mmag photometric calibration and be able to detect young SNe

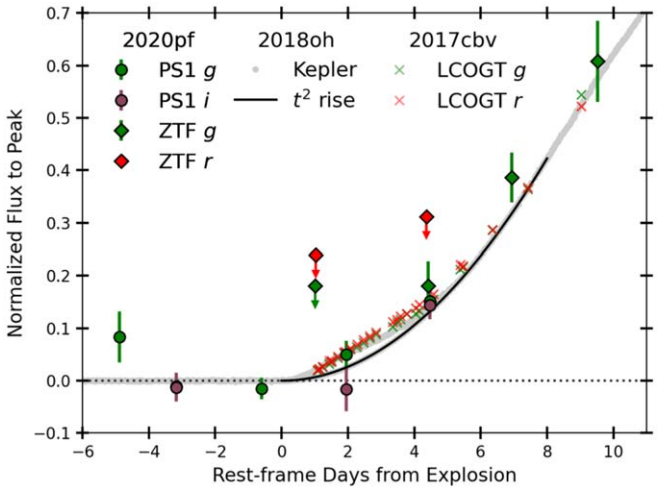

Figure 14. YSE (circles) and ZTF (diamonds) *gri* light curve of the relatively distant ($z = 0.095$) SN Ia SN 2020pf covering the time of explosion. We detect SN 2020pf 2 days after explosion. For comparison, we show the best-fit t^2 rising light curve, as well as early flux-excess SNe Ia SN 2017cbv and SN 2018oh (crosses and gray points, respectively; Hosseinzadeh et al. 2017; Dimitriadis et al. 2019a).

~1 day before they are detectable by other all-sky time-domain surveys. The oversampled Pan-STARRS PSF may make it easier to discover transients at the centers of galaxies.

YSE's data sets are yielding new insights into transient physics and are complementary to other ongoing surveys. YSE's multiwavelength light curves and our team's follow-up spectroscopy are forming a rich data set that will improve our understanding of the time-domain universe and prepare the community for the forthcoming Rubin Observatory and its Legacy Survey of Space and Time.

We thank S. Jha, R. Kirshner, K. Maguire, A. Riess, B. Schmidt, and D. Scolnic for discussion about survey strategy. We thank J. Nunez for help and useful discussions involving the YSE-PZ transient management system and E. Strasburger and J. Johnson for help with spectroscopic follow-up observations. We also thank the anonymous referee for their helpful suggestions to improve the manuscript.

D.O.J. acknowledges support from a Gordon and Betty Moore Foundation postdoctoral fellowship at the University of California, Santa Cruz. D.O.J., K.D.A., and K.D.F. also acknowledge support provided by NASA Hubble Fellowship grants HST-HF2-51462.001, HST-HF2-51403.001, and HST-HF2-51391.001-A, respectively, which are awarded by the Space Telescope Science Institute, operated by the Association of Universities for Research in Astronomy, Inc., for NASA, under contract NAS5-26555. The UCSC team is supported in part by NASA grants NNG17PX03C, 80NSSC19K1386, and 80NSSC20K0953; NSF grants AST-1518052, AST-1815935, and AST-1911206; the Gordon & Betty Moore Foundation; the Heising-Simons Foundation; and a fellowship from the David and Lucile Packard Foundation to R.J.F. D.A.C. and M.R.S. are supported by the National Science Foundation Graduate Research Fellowship Program Under grant Nos. DGE-1339067 and DGE-1842400, respectively. E.R.-R. is supported by the Heising-Simons Foundation and NSF (AST-1852393 and AST-1911206). E.R.-R. and H.P. are supported by the Danish National Research Foundation (DNRF132). H.P. is also indebted to the Hong Kong government (GRF grant HKU27305119) for support.

W.J.-G. is supported by the National Science Foundation Graduate Research Fellowship Program under grant No. DGE-1842165 and the IDEAS Fellowship Program at Northwestern University. C.D.K. acknowledges support through NASA grants in support of Hubble Space Telescope program AR-16136. The computations in this paper were aided by the University of Chicago Research Computing Center. R.M. acknowledges partial support by the National Science Foundation under award Nos. AST-1909796 and AST-1944985 and by the Heising-Simons Foundation under grant No. 2018-0911. R.M. is a CIFAR Azrieli Global Scholar in the Gravity & the Extreme Universe Program (2019) and an Alfred P. Sloan Fellow in Physics (2019).

This work was supported by a VILLUM FONDEN Investigator grant to J.H. (project No. 16599) and two Villum Young Investor Grants to C.G. and C.G. (10123 and 25501).

G.N. and K.D.F are grateful for support from the University of Illinois at Urbana-Champaign. D.C. is supported by the Center for Astrophysical Surveys at NCSA through the Illinois Survey Science Postdoctoral Fellowship. A.G. is supported by the National Science Foundation Graduate Research Fellowship Program under grant No. DGE1746047. A.G. and P.D.A. are supported by the Center for Astrophysical Surveys as Illinois Survey Science Graduate Fellows. A.G. additionally acknowledges support from the Illinois Distinguished Fellowship. A.E.'s work was supported by a 2019 Physics & Astronomy Student Travel Grant from the Council for Undergraduate Research. The computations in this paper made extensive use of the Illinois Campus Cluster and facilities at the National Center for Supercomputing Applications at UIUC.

Parts of this research were supported by the Australian Research Council Centre of Excellence for All Sky Astrophysics in 3 Dimensions (ASTRO 3D), through project No. CE170100013.

S.J.S. and K.W.S. are supported by STFC grants ST/P000312/1, ST/S006109/1 and ST/T000198/1.

A.H. is supported by Future Investigators in NASA Earth and Space Science and Technology (FINESST) award No. 80NSSC19K1422.

M.R.D. acknowledges support from the NSERC through grant RGPIN-2019-06186, the Canada Research Chairs Program, the Canadian Institute for Advanced Research (CIFAR), and the Dunlap Institute at the University of Toronto.

This project has received funding from the European Union's Horizon 2020 research and innovation program under the Marie Sklodowska-Curie grant agreement No. 891744 to S.I.R. Additionally, S.I.R. gratefully acknowledges support from the Independent Research Fund Denmark via grant Nos. DFF 4002-00275 and 8021-00130.

The Pan-STARRS1 Surveys (PS1) and the PS1 public science archive have been made possible through contributions by the Institute for Astronomy, the University of Hawaii, the Pan-STARRS Project Office, the Max-Planck Society and its participating institutes, the Max Planck Institute for Astronomy, Heidelberg and the Max Planck Institute for Extraterrestrial Physics, Garching, Johns Hopkins University, Durham University, the University of Edinburgh, the Queen's University Belfast, the Harvard-Smithsonian Center for Astrophysics, the Las Cumbres Observatory Global Telescope Network Incorporated, the National Central University of Taiwan, the Space Telescope Science Institute, the National Aeronautics and Space Administration under grant No. NNX08AR22G issued through the

Planetary Science Division of the NASA Science Mission Directorate, the National Science Foundation grant No. AST-1238877, the University of Maryland, Eotvos Lorand University (ELTE), the Los Alamos National Laboratory, and the Gordon and Betty Moore Foundation.

Some of the data presented herein were obtained at the W. M. Keck Observatory, which is operated as a scientific partnership among the California Institute of Technology, the University of California, and the National Aeronautics and Space Administration. The Observatory was made possible by the generous financial support of the W. M. Keck Foundation. The authors wish to recognize and acknowledge the very significant cultural role and reverence that the summit of Maunakea has always had within the indigenous Hawaiian community. We are most fortunate to have the opportunity to conduct observations from this mountain.

Based on observations obtained with the Samuel Oschin 48-inch Telescope at the Palomar Observatory as part of the Zwicky Transient Facility project. ZTF is supported by the National Science Foundation under grant No. AST-1440341 and a collaboration including Caltech, IPAC, the Weizmann Institute for Science, the Oskar Klein Center at Stockholm University, the University of Maryland, the University of Washington, Deutsches Elektronen-Synchrotron and Humboldt University, Los Alamos National Laboratories, the TANGO Consortium of Taiwan, the University of Wisconsin at Milwaukee, and Lawrence Berkeley National Laboratories. Operations are conducted by COO, IPAC, and UW.

We acknowledge the use of public data from the Neil Gehrels Swift Observatory data archive.

This research has made use of the NASA/IPAC Extragalactic Database (NED), which is operated by the Jet Propulsion Laboratory, California Institute of Technology, under contract with the National Aeronautics and Space Administration.

Appendix A
YSE Survey Simulation Variants and Methodology

To estimate SN discovery statistics from YSE, we used the SNANA simulation software (Kessler et al. 2010). SNANA generates catalog-based simulations that use real survey noise properties, detection efficiencies, SN rates, and luminosity functions, as well as the transient SED models used for the PLAsTiCC SN classification challenge (Kessler et al. 2019; Malz et al. 2019). We base the YSE simulations on simulations that were originally generated for the Foundation Supernova Survey and used for the cosmological parameter measurements in Jones et al. (2019). Because Foundation took predominantly 15 s exposures, we were able to generate an accurate YSE survey realization simply by scaling the exposure times to match the 5σ detection limits shown in Figure 2. This may introduce small errors in the relation between S/N and brightness, but these should be negligible as our analysis focuses on the number of detected SNe in the simulations (with the exception of cosmologically useful SNe Ia in Table 5, which may scale up or down slightly depending on the true survey noise properties).

The PLAsTiCC transient SED models are described in detail in Kessler et al. (2019). We do not simulate any variable sources (e.g., stars and AGNs) or purely theoretical models (e.g., pair-instability SNe or cosmic strings). However, we simulate the full range of available SN Ia and CC SN subtypes, as well as SNe Iax, Ca-rich transients, and intermediate-luminosity optical transients (ILOTs). The PLAsTiCC models come from a wide variety of sources; we note that at early times in particular they are based on scant observational data.

For the simulated SN rates, we again follow PLAsTiCC, which uses SN Ia rates from Dilday et al. (2008),

$$R_{\rm Ia}(z) = 2.5 \times 10^{-5}(1+z)^{1.5}\ {\rm yr}^{-1}\,{\rm Mpc}^{-3}\ (z < 1), \quad \text{(A1)}$$

while CC SN rates are from Strolger et al. (2015),

$$R_{\rm CC}(z) = 5.0 \times 10^{-5}(1+z)^{4.5}\ {\rm yr}^{-1}\,{\rm Mpc}^{-3}\ (z < 1). \quad \text{(A2)}$$

In most cases, normalization of the rates for different CC SN and SN Ia subtypes are given by the volume-limited measurements of Li et al. (2011b), but Kessler et al. (2019) list a few exceptions for peculiar events. Kessler et al. (2019) also describe the adopted redshift-dependent rates of peculiar classes of events. While the PLAsTiCC models and SNANA simulations suffer from a number of uncertainties in both the underlying models and the rates and luminosity functions of both rare and relatively common SN subtypes, PLAsTiCC is the most reliable currently available compilation combining rates, luminosity functions, and spectrophotometric transient models (however, see Vincenzi et al. 2019 for a recent update to a number of CC SN templates).

As a consistency check, we integrate these rates over our expected 1512 $\deg^2$ survey area and within volumes where we would expect to discover nearly every SN given the survey depth. Assuming 24% loss for detector masking and an additional 30% for weather, we predict a discovery rate of ~2300 SNe Ia per year to a distance of 1 Gpc and 76 CC SNe per year to a distance of 250 Mpc, distances corresponding to where a 27 s PS1 exposure should be sufficiently deep to detect nearly all SNe Ia and CC SNe. Our baseline simulation predicts that we should detect 1840 SNe Ia per year within 1 Gpc and 116 CC SN per year within 250 Mpc, consistent with these estimated numbers, with the increase in CC SNe likely due to the longer duration of many of these events.

We conservatively assume 24% masking of the GPC1 and GPC2 cameras, which will likely give a slight underestimate of the true SN yields, and the area shown in Table 5 includes these losses. Per-month estimates of weather loss are taken from PS1 data from the summit of Haleakala between 2010 and 2014 and are directly included in the simulation to account for correlations in downtime. We also varied the simulated survey depth as a function of lunar phase to match what we observe from Foundation data and the 3π survey; *gri* depths are estimated to vary by approximately 1.0, 0.7, and 0.2 mag between dark time and bright time, while z depths are assumed to remain constant. Typical night-to-night variation in depth is included. We also simulated an approximate ZTF survey by assuming an average depth of 21.1 mag in dark time that again varies to the same degree with moon phase as PS1, and we assumed that ZTF observations (when simulated Palomar and Haleakala weather allows) will always take place 21 hr after YSE observations. ZTF weather is estimated from monthly averages of weather loss at Palomar from the first year of ZTF observations.

A small number of second-order effects are not included in these simulations. First, we do not include loss due to the Pan-STARRS moon avoidance angle (30°–35°) in the simulations. Because we prioritize fields far from the ecliptic, this loss can usually be limited to approximately 5 days per month depending on the field. We also do not simulate the changing of the telescope position angle, which changes the location of masked pixels on the sky and is effectively a 20% weather-like

Table 5
Survey Strategy Comparisons for YSE

Filters[b]	Survey Parameters			SN Discoveries per Year			Young SNe per Year		Ia Cosmology[a]	
	Exp. (s)	$N_{\rm filt}$/day	Survey Area[c]	$z_{\rm med}$	$N_{\rm Ia}$	$N_{\rm CC}$	$N(\leqslant 2$ days)	$N(\leqslant 3$ days)	$z_{\rm med}$	$N_{\rm Ia}$/yr
Nominal Strategy										
$gr+gi$	27	2	1149 deg^2	0.19	4088	1063	4	28	0.12	812
Varying Exposure Times										
$gr+gi$	15	2	1679 deg^2	0.16	3463	817	2	25	0.11	759
$gr+gi$	20	2	1409 deg^2	0.17	3700	910	0	24	0.11	760
$gr+gi$	25	2	1213 deg^2	0.19	4119	1050	3	34	0.12	841
$gr+gi$	30	2	1065 deg^2	0.20	4151	1061	8	35	0.13	843
$gr+gi$	35	2	949 deg^2	0.21	4057	1092	3	25	0.14	770
Varying Number of Filters										
$gri+riz$	27	3	766 deg^2	0.20	3059	778	3	23	0.14	783
$griz$	27	4	575 deg^2	0.20	2367	643	1	13	0.15	649
Blue/Red Strategies										
gr	27	2	1149 deg^2	0.19	3960	1042	2	28	0.11	534
$ri+rz$	27	2	1149 deg^2	0.20	4287	1128	6	20	0.12	20[d]

Notes.
[a] Number of predicted cosmologically useful SNe Ia after applying standard selection criteria (Scolnic et al. 2018) and requiring total distance modulus uncertainty (including intrinsic dispersion) <0.15 mag.
[b] These filter combinations are for dark time; in bright time, we simulate combinations of *ri* and *rz* for all two-filter survey strategies owing to limited filter options that would achieve reasonable depths. In the case of three and four filters per day, the same strategies are used for both bright- and dark-time observations. The "*gr*+*gi*" sequence indicates that our survey design alternates these two-filter combinations with the full sequence repeating every 6 days.
[c] Area *after* assuming 24% masking of the GPC detectors per epoch.
[d] The small number is largely because SALT2 does not include the rest-frame *iz* bands in light-curve fitting.

reduction in the sampling of light curves (but *not* the area on sky). Finally, though fields will typically be observed for approximately 4–6 months per year, we do not include edge effects from rising or setting fields. We also do not simulate the Virgo 1-day survey. However, none of these effects should cause substantial reductions in the numbers or demographics of simulated SNe, which are our primary goals in this section.

The nominal survey strategy, along with several alternate strategies considered by our team, is shown in Table 5. We caution that some of the numbers, particularly discoveries of young SNe, are affected by small number statistics. Due to the limited filter choices during bright time to avoid the drastic reduction in *g*-band depth, we simulated an $ri+rz$ filter sequence during bright time for all two-filter survey designs. We found that as exposure time increases, the predicted number of SN discoveries also tends to increase but begins to flatten after 25 s, which is unsurprising given the volume as a function of exposure time shown in Figure 2. Choosing lower exposure times increases the number of transient discoveries for which we can obtain spectroscopic follow-up observations, while higher exposure time increases the total number of transients. We decided on a survey with two filters per epoch because the survey designs featuring three and four filters per epoch would be very valuable for some science cases but would substantially reduce the transient discovery volume. Finally, a blue-focused survey would probe a more similar discovery space to other ongoing surveys such as ZTF, while a red-focused survey would be expected to reduce the number of young SNe discovered, as these are expected to be blue. For these reasons, we chose a two-filter survey with a $gr+gi$ filter sequence during bright time with exposure times in each band of 27 s.

Appendix B
Components of the Field Selection Metric

The total YSE field selection metric m is computed from the following equation:

$$m = m_{\rm MW} \times m_d + m_z + m_{\rm DECaLS} + m_{ng} + m_f + m_e. \quad \text{(B1)}$$

The metric is computed from individual metrics, including the MW $E(B-V)$ from Schlafly & Finkbeiner (2011) ($m_{\rm MW}$), the combined depths from SDSS, Pan-STARRS 3π and MDS (m_d), the number of galaxies with measured redshifts (m_z), coverage from DECaLS ($m_{\rm DECaLS}$; Dey et al. 2019), the number of nearby galaxies m_{ng}, follow-up capability from Chile (m_f), and proximity to the ecliptic plane (m_e).

Each of these individual metrics is parameterized and scaled to ensure reasonable weights and a final range from 0 to 1. $m_{\rm MW}$ is set to zero for MW $E(B-V)$ greater than 0.2 and is proportional to the inverse extinction $[1+E(B-V)]^{-1}$. The depth metric m_d uses *r*-band depths from 20.5 ($m_d=0$) to 22.5 mag ($m_d=1$) scaled linearly; fields with PS1 MDS coverage are given a metric of 1, and the depth of either 3π or SDSS for non-MDS regions of sky is used depending on which is deeper (typically PS1, except for Stripe 82). For the nearby galaxies metric m_{ng}, we weight by the number of galaxies at <150, <40, <20, and <10 Mpc from the NASA/IPAC Extragalactic Database (NED) and combine each of these sets, e.g., galaxies at <10 Mpc contribute to the number of galaxies in all four maps and therefore have four times the

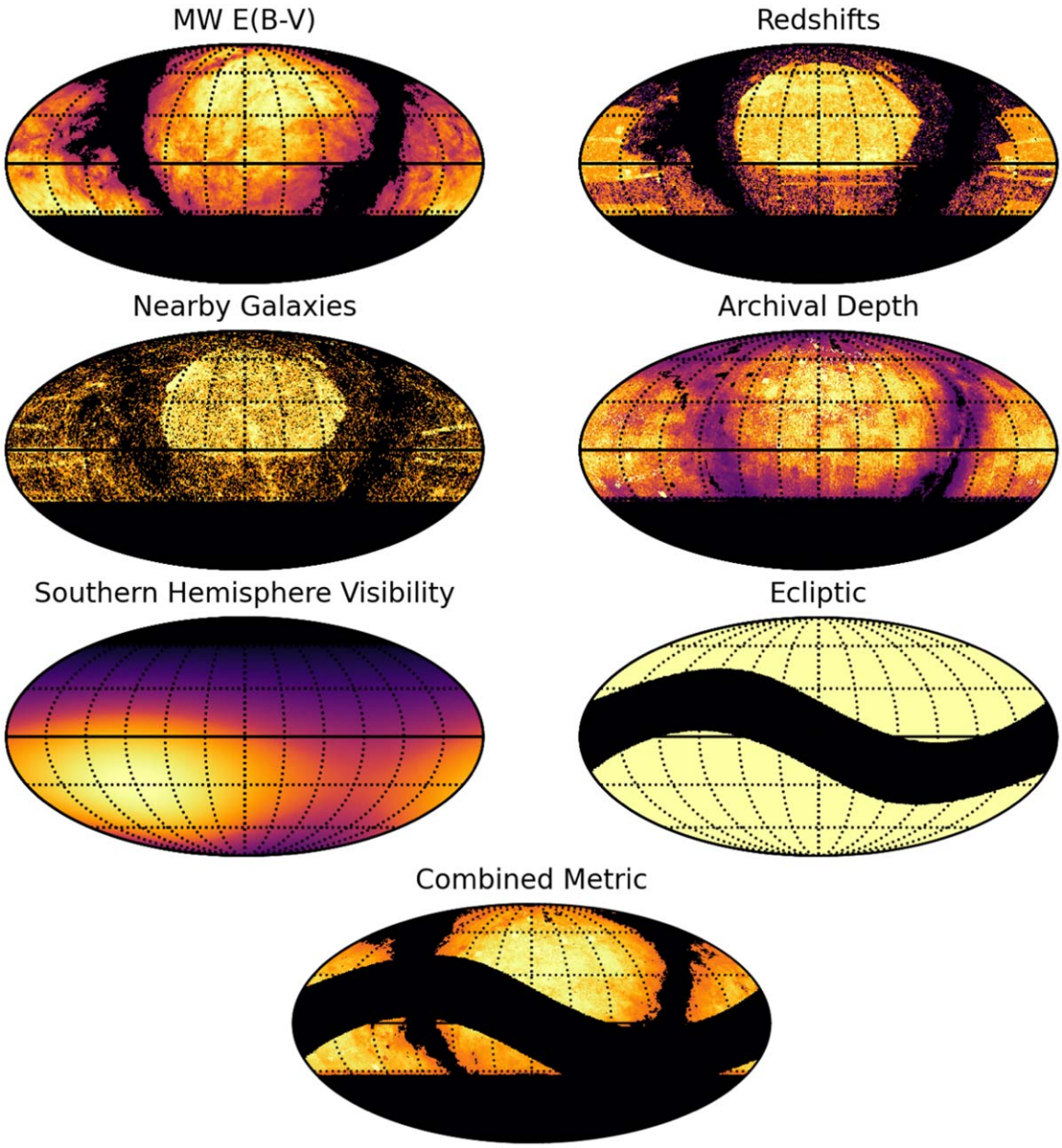

Figure 15. Components of the YSE field selection metric (top six panels) and combined metric map (bottom panel), with lighter colors corresponding to higher values of the metric. We note that a number of the input maps shown here are restricted to the 3π coverage area ($\delta > -30°$). We also prioritize the amount of HST exposure time, particularly interesting galaxies/clusters, and fields with newly discovered SNe from other surveys, but we do not formally include these in the metric. High-priority fields that do not pass our cut on proximity to the ecliptic are sometimes included in YSE.

effective weight of 150 Mpc galaxies. The nearby galaxies metric is added to the redshifts metric m_z, which is the number of redshifts from the combination of SDSS and NED. The resulting map is clipped at the 98th percentile to reduce the influence of large outliers. The DECaLS depth metric $m_{\rm DECaLS}$ is computed in the same manner as m_d but given half the weight as the other surveys, and not multiplied by the MW $E(B-V)$, given its predominantly z-band coverage. The follow-up observation metric m_f is arbitrarily determined as the product of the air mass and hours of observation per night from La Silla observatory in Chile averaged over a year. Most of the high-metric fields are in the Northern Hemisphere, and this choice weights YSE survey fields for which spectroscopic follow-up observations from Chile are possible. Finally, unless a field is of particular scientific interest, we exclude those fields within 20 deg of the ecliptic plane; due to the Pan-STARRS moon avoidance angle of 30 deg, fields near the ecliptic may have 8- to 10-day gaps in their light curves. The metric map is then normalized between 0 and 1.

The individual metric quantities and the final map are shown in Figure 15.

ORCID iDs

D. O. Jones https://orcid.org/0000-0002-6230-0151
G. Narayan https://orcid.org/0000-0001-6022-0484
J. Hjorth https://orcid.org/0000-0002-4571-2306
M. E. Huber https://orcid.org/0000-0003-1059-9603
P. D. Aleo https://orcid.org/0000-0002-6298-1663

K. D. Alexander https://orcid.org/0000-0002-8297-2473
K. Auchettl https://orcid.org/0000-0002-4449-9152
V. F. Baldassare https://orcid.org/0000-0003-4703-7276
S. H. Bruun https://orcid.org/0000-0002-5369-6094
K. C. Chambers https://orcid.org/0000-0001-6965-7789
D. Chatterjee https://orcid.org/0000-0003-0038-5468
D. L. Coppejans https://orcid.org/0000-0001-5126-6237
D. A. Coulter https://orcid.org/0000-0003-4263-2228
L. DeMarchi https://orcid.org/0000-0003-4587-2366
G. Dimitriadis https://orcid.org/0000-0001-9494-179X
M. R. Drout https://orcid.org/0000-0001-7081-0082
A. Engel https://orcid.org/0000-0003-2348-483X
K. D. French https://orcid.org/0000-0002-4235-7337
A. Gagliano https://orcid.org/0000-0003-4906-8447
C. Gall https://orcid.org/0000-0002-8526-3963
T. Hung https://orcid.org/0000-0002-9878-7889
L. Izzo https://orcid.org/0000-0001-9695-8472
W. V. Jacobson-Galán https://orcid.org/0000-0003-1103-3409
C. D. Kilpatrick https://orcid.org/0000-0002-5740-7747
H. Korhonen https://orcid.org/0000-0003-0529-1161
R. Margutti https://orcid.org/0000-0003-4768-7586
S. I. Raimundo https://orcid.org/0000-0002-6248-398X
E. Ramirez-Ruiz https://orcid.org/0000-0003-2558-3102
A. Rest https://orcid.org/0000-0002-4410-5387
C. Rojas-Bravo https://orcid.org/0000-0002-7559-315X
S. J. Smartt https://orcid.org/0000-0002-8229-1731
K. W. Smith https://orcid.org/0000-0001-9535-3199
G. Terreran https://orcid.org/0000-0003-0794-5982
Q. Wang https://orcid.org/0000-0001-5233-6989
R. Wojtak https://orcid.org/0000-0001-9666-3164
A. Agnello https://orcid.org/0000-0001-9775-0331
Z. Ansari https://orcid.org/0000-0002-4775-9685
N. Arendse https://orcid.org/0000-0001-5409-6480
P. K. Blanchard https://orcid.org/0000-0003-0526-2248
D. Brethauer https://orcid.org/0000-0001-6415-0903
J. S. Bright https://orcid.org/0000-0002-7735-5796
T. J. L. de Boer https://orcid.org/0000-0001-5486-2747
S. A. Dodd https://orcid.org/0000-0002-3696-8035
J. R. Fairlamb https://orcid.org/0000-0002-2833-2344
C. Grillo https://orcid.org/0000-0002-5926-7143
A. Hajela https://orcid.org/0000-0003-2349-101X
C. Hede https://orcid.org/0000-0001-7666-1874
A. N. Kolborg https://orcid.org/0000-0001-7364-4964
J. A. P. Law-Smith https://orcid.org/0000-0001-8825-4790
C.-C. Lin https://orcid.org/0000-0002-7272-5129
E. A. Magnier https://orcid.org/0000-0002-7965-2815
K. Malanchev https://orcid.org/0000-0001-7179-7406
D. Matthews https://orcid.org/0000-0002-4513-3849
B. Mockler https://orcid.org/0000-0001-6350-8168
D. Muthukrishna https://orcid.org/0000-0002-5788-9280
Y.-C. Pan https://orcid.org/0000-0001-8415-6720
H. Pfister https://orcid.org/0000-0003-0841-5182
D. K. Ramanah https://orcid.org/0000-0002-6029-7163
S. Rest https://orcid.org/0000-0002-3825-0553
A. Sarangi https://orcid.org/0000-0002-9820-679X
S. L. Schrøder https://orcid.org/0000-0003-1735-8263
C. Stauffer https://orcid.org/0000-0001-8769-4591
M. C. Stroh https://orcid.org/0000-0002-3019-4577
K. L. Taggart https://orcid.org/0000-0002-5748-4558
S. Tinyanont https://orcid.org/0000-0002-1481-4676
R. J. Wainscoat https://orcid.org/0000-0002-1341-0952

References

Abbott, B. P., Abbott, R., Abbott, T. D., et al. 2017, PhRvL, 119, 161101
Abbott, T. M. C., Abdalla, F. B., Allam, S., et al. 2018, ApJS, 239, 18
Abbott, T. M. C., Allam, S., Andersen, P., et al. 2019, ApJL, 872, L30
Ackley, K., Amati, L., Barbieri, C., et al. 2020, A&A, 643, A113
Aldering, G., Adam, G., Antilogus, P., et al. 2002, Proc. SPIE, 4836, 61
Aldering, G., Humphreys, R. M., & Richmond, M. 1994, AJ, 107, 662
Alexander, K. D., van Velzen, S., Horesh, A., & Zauderer, B. A. 2020, SSRv, 216, 81
Angus, C. R., Auchettl, K., Hjorth, J., et al. 2020, TNSAN, 2020-128
Arcavi, I., Gal-Yam, A., Yaron, O., et al. 2011, ApJL, 742, L18
Astier, P., Guy, J., Regnault, N., et al. 2006, A&A, 447, 31
Auchettl, K., Guillochon, J., & Ramirez-Ruiz, E. 2017, ApJ, 838, 149
Baldassare, V. F., Geha, M., & Greene, J. 2018, ApJ, 868, 152
Baldassare, V. F., Geha, M., & Greene, J. 2020, ApJ, 896, 10
Baldeschi, A., Miller, A., Stroh, M., Margutti, R., & Coppejans, D. L. 2020, ApJ, 902, 60
Baltay, C., Rabinowitz, D., Hadjiyska, E., et al. 2013, PASP, 125, 683
Barris, B. J., Tonry, J. L., Blondin, S., et al. 2004, ApJ, 602, 571
Becker, A. C., Wittman, D. M., Boeshaar, P. C., et al. 2004, ApJ, 611, 418
Bellm, E. C. 2016, PASP, 128, 084501
Bellm, E. C., Kulkarni, S. R., Barlow, T., et al. 2019a, PASP, 131, 068003
Bellm, E. C., Kulkarni, S. R., Graham, M. J., et al. 2019b, PASP, 131, 018002
Bellovary, J. M., Cleary, C. E., Munshi, F., et al. 2019, MNRAS, 482, 2913
Bernstein, J. P., Kessler, R., Kuhlmann, S., et al. 2012, ApJ, 753, 152
Betoule, M., Kessler, R., Guy, J., et al. 2014, A&A, 568, A22
Bloom, J. S., Giannios, D., Metzger, B. D., et al. 2011, Sci, 333, 203
Bloom, J. S., Richards, J. W., Nugent, P. E., et al. 2012, PASP, 124, 1175
Bond, H. E., Bedin, L. R., Bonanos, A. Z., et al. 2009, ApJL, 695, L154
Boone, K. 2019, AJ, 158, 257
Boruah, S. S., Hudson, M. J., & Lavaux, G. 2020, MNRAS, 498, 2703
Brout, D., Sako, M., Scolnic, D., et al. 2019a, ApJ, 874, 106
Brout, D., Scolnic, D., Kessler, R., et al. 2019b, ApJ, 874, 150
Bruch, R., Nordin, J., Schulze, S., et al. 2020a, TNSAN, 2020-136
Bruch, R., Schulze, S., & Gal-Yam, A. 2020b, TNSCR, 2020-2170
Burns, C. R., Stritzinger, M., Phillips, M. M., et al. 2011, AJ, 141, 19
Butler, N. R., & Bloom, J. S. 2011, AJ, 141, 93
Campana, S., Mangano, V., Blustin, A. J., et al. 2006, Natur, 442, 1008
Cao, Y., Kulkarni, S. R., Howell, D. A., et al. 2015, Natur, 521, 328
Chambers, K. C., Magnier, E. A., Metcalfe, N., et al. 2016, arXiv:1612.05560
Chomiuk, L., Chornock, R., Soderberg, A. M., et al. 2011, ApJ, 743, 114
Chomiuk, L., Soderberg, A. M., Moe, M., et al. 2012, ApJ, 750, 164
Chornock, R., Berger, E., Gezari, S., et al. 2014, ApJ, 780, 44
Coulter, D. A., Foley, R. J., Kilpatrick, C. D., et al. 2017, Sci, 358, 1556
Dark Energy Survey Collaboration, Abbott, T., Abdalla, F. B., et al. 2016, MNRAS, 460, 1270
De, K., Hankins, M. J., Kasliwal, M. M., et al. 2020a, PASP, 132, 025001
De, K., Kasliwal, M. M., Polin, A., et al. 2019, ApJL, 873, L18
De, K., Kasliwal, M. M., Tzanidakis, A., et al. 2020b, arXiv:2004.09029
Dey, A., Schlegel, D. J., Lang, D., et al. 2019, AJ, 157, 168
Dilday, B., Kessler, R., Frieman, J. A., et al. 2008, ApJ, 682, 262
Dimitriadis, G., Angus, C., Narayan, G., et al. 2020a, ATel, 13768
Dimitriadis, G., Foley, R. J., Rest, A., et al. 2019a, ApJL, 870, L1
Dimitriadis, G., Rojas-Bravo, C., Kilpatrick, C. D., et al. 2019b, ApJL, 870, L14
Dimitriadis, G., Siebert, M. R., Taggart, K., Tinyanont, S., & Foley, R. J. 2020b, TNSCR, 2020-2840
Drake, A. J., Djorgovski, S. G., Mahabal, A., et al. 2009, ApJ, 696, 870
Drout, M. R., Chornock, R., Soderberg, A. M., et al. 2014, ApJ, 794, 23
Drout, M. R., Piro, A. L., Shappee, B. J., et al. 2017, Sci, 358, 1570
Duev, D. A., Mahabal, A., Masci, F. J., et al. 2019, MNRAS, 489, 3582
Elias-Rosa, N., Pastorello, A., Benetti, S., et al. 2016, MNRAS, 463, 3894
Evans, R. 1994, PASAu, 11, 7
Fausnaugh, M. M., Vallely, P. J., Kochanek, C. S., et al. 2019, arXiv:1904.02171
Filippenko, A. V. 1992, in ASP Conf. Ser. 103, Robotic Telescopes in the 1990s, ed. A. V. Filippenko (San Francisco, CA: ASP), 55
Filippenko, A. V. 2005, in ASP Conf. Ser. 332, The Fate of the Most Massive Stars, ed. R. Humphreys & K. Stanek (San Francisco, CA: ASP), 34
Foley, R. J., Berger, E., Fox, O., et al. 2011, ApJ, 732, 32
Foley, R. J., Challis, P. J., Chornock, R., et al. 2013, ApJ, 767, 57
Foley, R. J., Chornock, R., Filippenko, A. V., et al. 2009, AJ, 138, 376
Foley, R. J., & Mandel, K. 2013, ApJ, 778, 167
Foley, R. J., Narayan, G., Challis, P. J., et al. 2010, ApJ, 708, 1748

Foley, R. J., Scolnic, D., Rest, A., et al. 2018, MNRAS, 475, 193
Foley, R. J., Smith, N., Ganeshalingam, M., et al. 2007, ApJL, 657, L105
Foley, R. J., Van Dyk, S. D., Jha, S. W., et al. 2015, ApJL, 798, L37
Forster, F., Bauer, F. E., Galbany, L., et al. 2020, TNSTR, 2020-2150
Fremling, C., Ko, H., Dugas, A., et al. 2019, ApJL, 878, L5
Fremling, C., Miller, A. A., Sharma, Y., et al. 2020, ApJ, 895, 32
French, K. D., Wevers, T., Law-Smith, J., Graur, O., & Zabludoff, A. I. 2020, SSRv, 216, 32
Frieman, J. A., Bassett, B., Becker, A., et al. 2008, AJ, 135, 338
Gagliano, A., Narayan, G., Engel, A., & Carrasco Kind, M. 2020, arXiv:2008.09630
Galama, T. J., Vreeswijk, P. M., van Paradijs, J., et al. 1998, Natur, 395, 670
Gal-Yam, A. 2012, Sci, 337, 927
Gal-Yam, A. 2019, ARA&A, 57, 305
Gal-Yam, A., Arcavi, I., Ofek, E. O., et al. 2014, Natur, 509, 471
Ganeshalingam, M., Li, W., Filippenko, A. V., et al. 2010, ApJS, 190, 418
Gezari, S., Cenko, S. B., & Arcavi, I. 2017, ApJL, 851, L47
Gezari, S., Martin, D. C., Forster, K., et al. 2013, ApJ, 766, 60
Graur, O., Rodney, S. A., Maoz, D., et al. 2014, ApJ, 783, 28
Guillochon, J., Parrent, J., Kelley, L. Z., & Margutti, R. 2017, ApJ, 835, 64
Guy, J., Astier, P., Baumont, S., et al. 2007, A&A, 466, 11
Guy, J., Sullivan, M., Conley, A., et al. 2010, A&A, 523, A7
Hamuy, M., Maza, J., Phillips, M. M., et al. 1993, AJ, 106, 2392
Hamuy, M., Phillips, M. M., Suntzeff, N. B., et al. 2003, Natur, 424, 651
Hjorth, J., Sollerman, J., Møller, P., et al. 2003, Natur, 423, 847
Holoien, T. W.-S., Brown, J. S., Stanek, K. Z., et al. 2017, MNRAS, 471, 4966
Holoien, T. W. S., Huber, M. E., Shappee, B. J., et al. 2019, ApJ, 880, 120
Hönig, S. F., Watson, D., Kishimoto, M., et al. 2017, MNRAS, 464, 1693
Hosseinzadeh, G., Dauphin, F., Villar, V. A., et al. 2020, ApJ, 905, 93
Hosseinzadeh, G., Sand, D. J., Valenti, S., et al. 2017, ApJL, 845, L11
Hounsell, R., Scolnic, D., Foley, R. J., et al. 2018, ApJ, 867, 23
Howell, S. B., Sobeck, C., Haas, M., et al. 2014, PASP, 126, 398
Howlett, C., Robotham, A. S. G., Lagos, C. D. P., & Kim, A. G. 2017, ApJ, 847, 128
Huber, M., Chambers, K. C., Flewelling, H., et al. 2015, ATel, 7153
Hung, T., Foley, R. J., Ramirez-Ruiz, E., et al. 2020, ApJ, 903, 31
Hung, T., Gezari, S., Blagorodnova, N., et al. 2017, ApJ, 842, 29
Huterer, D., Shafer, D. L., Scolnic, D. M., & Schmidt, F. 2017, JCAP, 2017, 015
Izzo, L., Angus, C., Bruun, S., et al. 2020, TNSAN, 75
Jacobson-Galán, W. V., Margutti, R., Kilpatrick, C. D., et al. 2020a, ApJ, 898, 166
Jacobson-Galán, W. V., Polin, A., Foley, R. J., et al. 2020b, ApJ, 896, 165
Jiang, J.-A., Doi, M., Maeda, K., et al. 2017, Natur, 550, 80
Jiang, J.-a., Yasuda, N., Maeda, K., et al. 2020, ApJ, 892, 25
Jones, D. O., Riess, A. G., Scolnic, D. M., et al. 2018a, ApJ, 867, 108
Jones, D. O., Scolnic, D. M., Foley, R. J., et al. 2019, ApJ, 881, 19
Jones, D. O., Scolnic, D. M., Riess, A. G., et al. 2017, ApJ, 843, 6
Jones, D. O., Scolnic, D. M., Riess, A. G., et al. 2018b, ApJ, 857, 51
Kaiser, N., Aussel, H., Burke, B. E., et al. 2002, Proc. SPIE, 4836, 154
Kare, J. T., Pennypacker, C. R., Muller, R. A., et al. 1982, in Supernovae: A Survey of Current Research, ed. M. J. Rees & R. J. Stoneham (Dordrecht: Springer), 325
Kasliwal, M. M., Cannella, C., Bagdasaryan, A., et al. 2019, PASP, 131, 038003
Keller, S. C., Schmidt, B. P., Bessell, M. S., et al. 2007, PASA, 24, 1
Kelly, B. C., Bechtold, J., & Siemiginowska, A. 2009, ApJ, 698, 895
Kelly, P. L., Filippenko, A. V., Burke, D. L., et al. 2015, Sci, 347, 1459
Kessler, R., Bassett, B., Belov, P., et al. 2010, PASP, 122, 1415
Kessler, R., Becker, A. C., Cinabro, D., et al. 2009, ApJS, 185, 32
Kessler, R., Narayan, G., Avelino, A., et al. 2019, PASP, 131, 094501
Kilpatrick, C. D., & Foley, R. J. 2018, MNRAS, 481, 2536
Kilpatrick, C. D., Foley, R. J., Abramson, L. E., et al. 2017, MNRAS, 465, 4650
Kilpatrick, C. D., Foley, R. J., Drout, M. R., et al. 2018a, MNRAS, 473, 4805
Kilpatrick, C. D., Takaro, T., Foley, R. J., et al. 2018b, MNRAS, 480, 2072
Kim, A., Aldering, G., Antilogus, P., et al. 2019, BAAS, 51, 140
Kim, S.-L., Lee, C.-U., Park, B.-G., et al. 2016, JKAS, 49, 37
Kimura, Y., Yamada, T., Kokubo, M., et al. 2020, ApJ, 894, 24
Knop, R., Aldering, G., Deustua, S., et al. 1999, IAUC, 7128, 1
Kochanek, C. S. 2016, MNRAS, 461, 371
Kowal, C. T. 1968, AJ, 73, 1021
Kuijken, K., Heymans, C., Dvornik, A., et al. 2019, A&A, 625, A2
Kunkel, W., Madore, B., Shelton, I., et al. 1987, IAUC, 4316, 1
LaMassa, S. M., Cales, S., Moran, E. C., et al. 2015, ApJ, 800, 144
Law, N. M., Fors, O., Ratzloff, J., et al. 2015, PASP, 127, 234
Law, N. M., Kulkarni, S. R., Dekany, R. G., et al. 2009, PASP, 121, 1395
Leaman, J., Li, W., Chornock, R., & Filippenko, A. V. 2011, MNRAS, 412, 1419
Léget, P. F., Gangler, E., Mondon, F., et al. 2020, A&A, 636, A46
Leloudas, G., Chatzopoulos, E., Dilday, B., et al. 2012, A&A, 541, A129
Li, W., Bloom, J. S., Podsiadlowski, P., et al. 2011a, Natur, 480, 348
Li, W., Filippenko, A. V., Gates, E., et al. 2001, PASP, 113, 1178
Li, W., Leaman, J., Chornock, R., et al. 2011b, MNRAS, 412, 1441
Lipunov, V., Kornilov, V., Gorbovskoy, E., et al. 2010, AdAst, 2010, 349171
Lorimer, D. R., Bailes, M., McLaughlin, M. A., Narkevic, D. J., & Crawford, F. 2007, Sci, 318, 777
LSST Science Collaboration, Abell, P. A., Allison, J., et al. 2009, arXiv:0912.0201
Lunnan, R., Chornock, R., Berger, E., et al. 2013, ApJ, 771, 97
Lunnan, R., Chornock, R., Berger, E., et al. 2015, ApJ, 804, 90
MacLeod, C. L., Green, P. J., Anderson, S. F., et al. 2019, ApJ, 874, 8
MacLeod, C. L., Ivezić, Ž, Kochanek, C. S., et al. 2010, ApJ, 721, 1014
MacLeod, C. L., Ross, N. P., Lawrence, A., et al. 2016, MNRAS, 457, 389
MacLeod, M., Guillochon, J., & Ramirez-Ruiz, E. 2012, ApJ, 757, 134
Magnier, E. A., Sweeney, W. E., Chambers, K. C., et al. 2020, ApJS, 251, 5
Malz, A. I., Hložek, R., Allam, T. J., et al. 2019, AJ, 158, 171
Mandel, K. S., Thorp, S., Narayan, G., Friedman, A. S., & Avelino, A. 2020, arXiv:2008.07538
Maoz, D., & Graur, O. 2017, ApJ, 848, 25
Margutti, R., Milisavljevic, D., Soderberg, A. M., et al. 2014, ApJ, 780, 21
Margutti, R., Soderberg, A. M., Chomiuk, L., et al. 2012, ApJ, 751, 134
Marion, G. H., Brown, P. J., Vinkó, J., et al. 2016, ApJ, 820, 92
Masci, F. J., Laher, R. R., Rusholme, B., et al. 2019, PASP, 131, 018003
Mason, E., Diaz, M., Williams, R. E., Preston, G., & Bensby, T. 2010, A&A, 516, A108
Maza, J. 1980, in Proc. Texas Workshop, Type I Supernovae, ed. J. C. Wheeler (Austin, TX: University of Texas), 7
McBrien, O. R., Smartt, S. J., Huber, M. E., et al. 2021, MNRAS, 500, 4213
McCrum, M., Smartt, S. J., Kotak, R., et al. 2014, MNRAS, 437, 656
McCully, C., Jha, S. W., Foley, R. J., et al. 2014, Natur, 512, 54
Miknaitis, G., Pignata, G., Rest, A., et al. 2007, ApJ, 666, 674
Miller, A. A., Yao, Y., Bulla, M., et al. 2020, ApJ, 902, 47
Mockler, B., Guillochon, J., & Ramirez-Ruiz, E. 2019, ApJ, 872, 151
Möller, A., & de Boissière, T. 2020, MNRAS, 491, 4277
Mould, J., Cohen, J., Graham, J. R., et al. 1990, ApJL, 353, L35
Muthukrishna, D., Narayan, G., Mandel, K. S., Biswas, R., & Hložek, R. 2019, PASP, 131, 118002
Narayan, G., Axelrod, T., Holberg, J. B., et al. 2016, ApJ, 822, 67
Narayan, G., Foley, R. J., Berger, E., et al. 2011, ApJL, 731, L11
Narayan, G., Zaidi, T., Soraisam, M. D., et al. 2018, ApJS, 236, 9
Nicholl, M., Berger, E., Margutti, R., et al. 2017, ApJL, 845, L8
Nicholl, M., Smartt, S. J., Jerkstrand, A., et al. 2015, ApJL, 807, L18
Nicholls, C. P., Melis, C., Soszynski, I., et al. 2013, MNRAS, 431, L33
Nomoto, K., Kobayashi, C., & Tominaga, N. 2013, ARA&A, 51, 457
Norgaard-Nielsen, H. U., Hansen, L., Jorgensen, H. E., Aragon Salamanca, A., & Ellis, R. S. 1989, Natur, 339, 523
Ofek, E. O., Sullivan, M., Shaviv, N. J., et al. 2014, ApJ, 789, 104
Pastorello, A., Cappellaro, E., Inserra, C., et al. 2013, ApJ, 767, 1
Pastorello, A., Chen, T. W., Cai, Y. Z., et al. 2019, A&A, 625, L8
Pastorello, A., Smartt, S. J., Mattila, S., et al. 2007, Natur, 447, 829
Perets, H. B., Gal-Yam, A., Mazzali, P. A., et al. 2010, Natur, 465, 322
Perley, D. A., Fremling, C., Sollerman, J., et al. 2020, ApJ, 904, 35
Perlmutter, S. 1989, Particle Astrophysics: Forefront Experimental Issues (Singapore: World Scientific), 196
Perlmutter, S., Aldering, G., Goldhaber, G., et al. 1999, ApJ, 517, 565
Perlmutter, S., Gabi, S., Goldhaber, G., et al. 1997, ApJ, 483, 565
Phillips, M. M. 1993, ApJL, 413, L105
Pignata, G., Maza, J., Antezana, R., et al. 2009, in AIP Conf. Ser. 1111, Probing Stellar Populations Out of the Distant Universe, ed. G. Giobbi et al. (Melville, NY: AIP), 551
Piro, A. L., & Nakar, E. 2013, ApJ, 769, 67
Popovic, B., Scolnic, D., & Kessler, R. 2020, ApJ, 890, 172
Pskovskii, I. P. 1977, SvA, 21, 675
Quimby, R. M. 2006, PhD thesis, The Univ. Texas at Austin, TX
Quimby, R. M., Kulkarni, S. R., Kasliwal, M. M., et al. 2011, Natur, 474, 487
Refsdal, S. 1964, MNRAS, 128, 307
Reines, A. E., Condon, J. J., Darling, J., & Greene, J. E. 2020, ApJ, 888, 36
Rest, A., Scolnic, D., Foley, R. J., et al. 2014, ApJ, 795, 44
Richmond, M., Treffers, R. R., & Filippenko, A. V. 1993, PASP, 105, 1164
Richmond, M. W., Treffers, R. R., Filippenko, A. V., et al. 1994, AJ, 107, 1022
Riess, A. G., Filippenko, A. V., Challis, P., et al. 1998, AJ, 116, 1009

Riess, A. G., Macri, L. M., Hoffmann, S. L., et al. 2016, ApJ, 826, 56
Rigault, M., Brinnel, V., Aldering, G., et al. 2020, A&A, 644, A176
Rigault, M., Copin, Y., Aldering, G., et al. 2013, A&A, 560, A66
Rodney, S. A., Balestra, I., Bradac, M., et al. 2018, NatAs, 2, 324
Rodney, S. A., Riess, A. G., Strolger, L.-G., et al. 2014, AJ, 148, 13
Roman, M., Hardin, D., Betoule, M., et al. 2018, A&A, 615, A68
Ruan, J. J., Anderson, S. F., Cales, S. L., et al. 2016, ApJ, 826, 188
Runnoe, J. C., Cales, S., Ruan, J. J., et al. 2016, MNRAS, 455, 1691
Rust, B. W. 1974, PhD thesis, Oak Ridge National Lab., TN
Sako, M., Bassett, B., Becker, A. C., et al. 2018, PASP, 130, 064002
Sánchez-Sáez, P., Lira, P., Cartier, R., et al. 2019, ApJS, 242, 10
Sánchez-Sáez, P., Lira, P., Mejía-Restrepo, J., et al. 2018, ApJ, 864, 87
Sanders, N. E., Soderberg, A. M., Levesque, E. M., et al. 2012, ApJ, 758, 132
Saunders, C., Aldering, G., Antilogus, P., et al. 2018, ApJ, 869, 167
Scalzo, R. A., Yuan, F., Childress, M. J., et al. 2017, PASA, 34, e030
Schlafly, E. F., & Finkbeiner, D. P. 2011, ApJ, 737, 103
Schlafly, E. F., Finkbeiner, D. P., Jurić, M., et al. 2012, ApJ, 756, 158
Schmidt, B. P., Suntzeff, N. B., Phillips, M. M., et al. 1998, ApJ, 507, 46
Scolnic, D., Casertano, S., Riess, A., et al. 2015, ApJ, 815, 117
Scolnic, D. M., Jones, D. O., Rest, A., et al. 2018, ApJ, 859, 101
Shappee, B. J., Holoien, T. W. S., Drout, M. R., et al. 2019, ApJ, 870, 13
Shappee, B. J., Prieto, J. L., Grupe, D., et al. 2014, ApJ, 788, 48
Siebert, M. R., Dimitriadis, G., Polin, A., & Foley, R. J. 2020, ApJL, 900, L27
Siebert, M. R., Foley, R. J., Drout, M. R., et al. 2017, ApJL, 848, L26
Smartt, S. J., Chambers, K. C., Smith, K. W., et al. 2016, MNRAS, 462, 4094
Smartt, S. J., Eldridge, J. J., Crockett, R. M., & Maund, J. R. 2009, MNRAS, 395, 1409
Smartt, S. J., Valenti, S., Fraser, M., et al. 2015, A&A, 579, A40
Smith, K. W., Smartt, S. J., Young, D. R., et al. 2020, PASP, 132, 085002
Smith, M., Sullivan, M., D'Andrea, C. B., et al. 2016, ApJL, 818, L8
Smith, N. 2014, ARA&A, 52, 487
Smith, N., Chornock, R., Silverman, J. M., Filippenko, A. V., & Foley, R. J. 2010a, ApJ, 709, 856
Smith, N., Li, W., Foley, R. J., et al. 2007, ApJ, 666, 1116
Smith, N., Miller, A., Li, W., et al. 2010b, AJ, 139, 1451
Srivastav, S., Smartt, S. J., Leloudas, G., et al. 2020, ApJL, 892, L24
Stanek, K. Z., Matheson, T., Garnavich, P. M., et al. 2003, ApJL, 591, L17
Strolger, L.-G., Dahlen, T., Rodney, S. A., et al. 2015, ApJ, 813, 93
Taggart, K., & Perley, D. 2019, arXiv:1911.09112
Tanaka, M., Tominaga, N., Morokuma, T., et al. 2016, ApJ, 819, 5
Tanvir, N. R., Levan, A. J., González-Fernández, C., et al. 2017, ApJL, 848, L27
Thöne, C. C., de Ugarte Postigo, A., Leloudas, G., et al. 2017, A&A, 599, A129
Tonry, J. L. 2011, PASP, 123, 58
Tonry, J. L., Denneau, L., Heinze, A. N., et al. 2018, PASP, 130, 064505
Tonry, J. L., Stubbs, C. W., Lykke, K. R., et al. 2012, ApJ, 750, 99
Tucker, M. A., Shappee, B. J., & Wisniewski, J. P. 2019, ApJL, 872, L22
Valenti, S., Pastorello, A., Cappellaro, E., et al. 2009, Natur, 459, 674
Valenti, S., Sand, D. J., Yang, S., et al. 2017, ApJL, 848, L24
van der Walt, S., Crellin-Quick, A., & Bloom, J. 2019, JOSS, 4, 1247
Van Dyk, S. D., Peng, C. Y., King, J. Y., et al. 2000, PASP, 112, 1532
van Velzen, S., Gezari, S., Hammerstein, E., et al. 2021, ApJ, 908, 4
Villar, V. A., Berger, E., Miller, G., et al. 2019, ApJ, 884, 83
Villar, V. A., Hosseinzadeh, G., Berger, E., et al. 2020, ApJ, 905, 94
Vincenzi, M., Sullivan, M., Firth, R. E., et al. 2019, MNRAS, 489, 5802
Vincenzi, M., Sullivan, M., Graur, O., et al. 2020, arXiv:2012.07180
Wojtak, R., Hjorth, J., & Gall, C. 2019, MNRAS, 487, 3342
Woosley, S. E., Pinto, P. A., Martin, P. G., & Weaver, T. A. 1987, ApJ, 318, 664
York, D. G., Adelman, J., Anderson, J. E. J., et al. 2000, AJ, 120, 1579
Zauderer, B. A., Berger, E., Soderberg, A. M., et al. 2011, Natur, 476, 425
Zwicky, F. 1938, PASP, 50, 215